European Journal of Medicinal Chemistry 286 (2025) 117250

Contents lists available at ScienceDirect

European Journal of Medicinal Chemistry

journal homepage: www.elsevier.com/locate/ejmech

Research paper

Design, synthesis, and anti-liver fibrosis activity of novel non-steroidal vitamin D receptor agonists based on open-ring steroid scaffold

Fei Gao [1], Chun Guan [1], Nuo Cheng, Yichen Liu, Yue Wu, Bingyue Shi, Jiayi Huang, Sitong Li, Yu Tong, Yi Gao, Jiayi Liu, Cong Wang **, Can Zhang *

State Key Laboratory of Natural Medicines, Jiangsu Key Laboratory of Drug Discovery for Metabolic Diseases, Center of Advanced Pharmaceuticals and Biomaterials, China Pharmaceutical University, Nanjing, 211198, PR China

ARTICLE INFO

Keywords:
Vitamin D
Vitamin D receptor
Non-steroidal compounds
Anti-liver fibrosis

ABSTRACT

Vitamin D receptor (VDR) has emerged as a crucial target for the treatment of hepatic fibrosis, a condition characterized by excessive deposition of extracellular matrix (ECM) components leading to impaired liver function. Activation of VDR has been shown to inhibit the transformation of hepatic stellate cells (HSCs), which play a key role in the development of liver fibrosis, thus reducing ECM production. In this study, a series of 37 non-steroidal VDR agonists with novel scaffold were designed and synthesized utilizing the scaffold hopping strategy. Over one-third of these compounds demonstrated significant VDR affinity and agonistic activity. Among them, compound **E15** exhibited the highest VDR agonistic activity, showing promising results in vitro by effectively inhibiting HSC activation. Further in vivo assessments of **E15** in a carbon tetrachloride-induced murine model of liver fibrosis demonstrated significant anti-fibrotic activity. Histological analyses revealed a reduction in lesions, inflammatory cell infiltration, and collagen deposition. Concurrently, blood biochemical assays indicated decreased hepatic fibrosis markers and improved serum liver function indices. Notably, **E15** achieved these therapeutic effects without inducing hypercalcemia, a common adverse effect associated with VDR agonists such as calcipotriol. These findings underscore the potential of **E15** as a potent and safe therapeutic agent for the treatment of liver fibrosis.

1. Introduction

Vitamin D_3 (VD_3) functions as a prohormone that undergoes two hydroxylation reactions within the body to be converted into 1α,25-dihydroxyvitamin D_3 (calcitriol), the biologically active form of VD_3 [1]. This active form exerts a broad spectrum of physiological effects by binding to the vitamin D receptor (VDR) [2]. The VDR, a ligand-activated transcription factor, forms a heterodimer with the retinoid X receptor (RXR) upon activation. This VDR-RXR heterodimer subsequently recruits various cofactors to assemble a transcriptional complex that binds to vitamin D response elements (VDREs) on DNA, thereby regulating the expression of numerous genes [3–5]. Beyond its classical roles in calcium and phosphorus homeostasis, VDR influences cell proliferation, differentiation, and immune responses, linking it to diseases such as osteoporosis, cancer, and autoimmune disorders [6–8].

Recent research has elucidated a substantial association between VDR signaling and liver fibrosis. Initially, it has been observed that reduced plasma vitamin D levels are correlated with increased severity of liver fibrosis in patients with chronic liver disease. Moreover, vitamin D deficiency, which is prevalent among individuals with liver fibrosis, is linked to poorer prognostic outcomes [9–12]. Furthermore, clinical trials have indicated that vitamin D supplementation can ameliorate fibrosis markers in patients with chronic hepatitis C [13]. Complementing these clinical observations, in vitro studies and various animal models have demonstrated that 1α,25-dihydroxyvitamin D_3 and the VDR agonist calcipotriol can mitigate fibrosis markers [14–17]. Hepatic stellate cells (HSCs), which are the primary producers of fibrotic collagen, exhibit elevated levels of VDR expression [18,19]. Upon activation by its ligand, VDR in HSCs forms a VDR-RXR heterodimer that competitively binds to SMAD3 binding sites on chromatin. This binding inhibits the pro-fibrotic TGF-β/SMAD3 signaling pathway, thereby reducing the expression of fibrogenic genes [20–22]. These findings

* Corresponding author.
** Corresponding author.
E-mail addresses: wangcong@cpu.edu.cn (C. Wang), zhangcan@cpu.edu.cn (C. Zhang).
[1] These authors contributed equally to this work.

https://doi.org/10.1016/j.ejmech.2025.117250
Received 4 November 2024; Received in revised form 5 January 2025; Accepted 5 January 2025
Available online 9 January 2025
0223-5234/© 2025 Published by Elsevier Masson SAS.

collectively indicate that VDR agonists hold potential as therapeutic agents for the treatment of liver fibrosis.

Despite the diverse physiological functions of 1α,25-dihydroxyvitamin D_3 and its potential applications in treating various diseases, its therapeutic use is constrained by the side effect of hypercalcemia. Over the years, medicinal chemists have endeavored to dissociate its calcium-phosphorus regulatory functions from other physiological effects through structural modifications. Thousands of natural vitamin D analogs have been reported, and while some have significantly reduced hypercalcemic effects, they still pose a risk of hypercalcemia with long-term high-dose administration [23], rendering them unsuitable for the management of chronic diseases like liver fibrosis. The development of non-steroidal ligands represents a prevalent approach for the selective modulation of nuclear receptor functions. Prior research has identified two classes of non-steroidal VDR agonists, specifically compounds **15a** and **16i**, which have demonstrated efficacy in mitigating liver fibrosis symptoms in animal models without inducing hypercalcemia [24,25]. Despite these promising results, the anti-fibrotic activity of these compounds requires further optimization.

This study hypothesizes that enhancing the VDR agonist activity of these compounds could serve as an effective strategy for improving their anti-fibrotic efficacy, based on the underlying mechanisms of VDR-mediated anti-fibrotic effects. To develop more potent VDR agonists, we initially analyzed the binding modes of 1α,25-dihydroxyvitamin D_3 and the aforementioned non-steroidal VDR compounds with VDR. 1α,25-dihydroxyvitamin D_3 interacts with VDR through its A-ring, conjugated triene, and terminal tertiary alcohol side chain via hydrogen bonding and hydrophobic interactions with the H3, H5, and H12 helices, which are associated with the transactivation function of VDR [26,27]. These structural characteristics of 1α,25-dihydroxyvitamin D_3 may be essential for its transcriptional activity. In contrast, the hydroxyl groups present in the 1,2-diol or vicinal diol configurations of compounds **15a** and **16i** exhibit a lack of conformational restriction. The phenyl rings, employed to emulate the triene structure, are comparatively large and may induce steric clashes with amino acid residues within the H3 and H5 domains, thereby negatively impacting transcriptional activity. Furthermore, the structure-activity relationship of certain secosteroidal compounds indicates that the presence of a conjugated triene system and saturated C/D rings likely contributes to the manifestation of hypercalcemia [28,29]. Additionally, a class of Des-C-Ring and Aromatic-D-Ring Analogs of 1α,25-Dihydroxyvitamin D3 has been reported, which exhibit minimal elevation of serum calcium levels [30,31].

Taking these factors into account, we developed novel non-steroidal scaffolds by preserving elements of the natural VD structure, specifically avoiding the saturated C/D ring configuration, modifying the conjugated triene system, and maintaining the integrity of the A-ring. Utilizing the secosteroid structure of natural VD_3 as a basis, we implemented a scaffold-hopping strategy and synthesized 37 compounds through two iterative rounds of structural design. Among these synthesized compounds, **E15** demonstrated significantly enhanced VDR affinity and in vitro anti-fibrotic activity compared to the previously reported compounds **15a** and **16i**. In a CCl_4-induced mouse liver fibrosis model, **E15** effectively inhibited fibrosis progression without increasing blood calcium levels (see Fig. 1).

2. Result and discussion

2.1. Structural design

As illustrated in Fig. 2 and Table 1, during the initial phase of compound design, we employed the 1,2,3-cyclohexene triol fragment derived from shikimic acid to replicate the chair conformation of the A ring and the stereochemical configuration of the hydroxyl groups at positions 1 and 3, as observed in secosteroidal VDR agonists. Additionally, since the VD_3 metabolite 1α,2β,25$(OH)_3VD_3$ with a 2β-OH group demonstrates higher VDR affinity compared to 1α,25-dihydroxyvitamin D_3 [32], we hypothesize that incorporating the same 2β-OH group in our compound design could also result in compounds with high VDR affinity. To achieve this, we substituted the fully saturated C/D rings with a tetrahydronaphthalene fragment that possesses a certain degree of unsaturation. These two fragments were connected using trans double bond (**A1-A13**) or triple bond (**B1–B5**), creating a conjugated system different from the conjugated triene segment of secosteroidal VDR agonists, thus aiming to minimize the risk of hypercalcemia. Furthermore, this round explored the effects of types of aromatic rings, and the positions of these side chains on their biological activity (**C1–C2**). In the second round of compound design, a side chain was introduced at the meta position of the benzene ring to better fit the orientation of the compound within the cavity of the VDR ligand-binding domain. A semi-flexible modification was achieved by replacing the trans double bond with an ester bond (**E1-E9**). Additionally, a ring-opening scaffold-hopping strategy was employed to further increase the flexibility of the compound (**E10-E17**), promoting the formation of preferred conformations.

2.2. Chemistry

The synthetic route of compounds **A1-A13** and **C1–C2** is shown in Scheme 1. Compound **1** was esterified with methanol catalyzed by sulfoxide chloride and protected from the hydroxyl groups by the tert-butyldimethylsilyl group to yield intermediate **3**, which was reduced by DIBAL-H and then oxidized by manganese dioxide to yield intermediate **5**, which was subjected to Calvin alkyne synthesis to yield intermediate **6**. Intermediate **6** was then treated to a monovalent copper-catalyzed borylation reaction [33], yielding intermediate **7**. Intermediates **9a-9m** were created by introducing different side chains through a nucleophilic substitution reaction, and intermediate **7** was then reacted with intermediates **9a-9m** via Suzuki cross-coupling reaction to produce intermediates **10a-10m**, while intermediates **10f-10g** were reduced using a sodium borohydride/methanol system to produce intermediates **11a-11b**. Theoretically, this reduction generates a pair of diastereomers in a 1:1 ratio, due to the lack of stereoselectivity of the $NaBH_4$/MeOH system in this specific reaction. Finally, intermediates **10a-10m** and **11a-11b** were deprotected by TBAF, yielding the target compounds **A1-A13** and **C1–C2**.

The synthetic route of compounds **B1–B5** is shown in Scheme 2. Intermediate **6** was reacted with intermediates **9b-9d** and **9n-9o** via Sonogashira cross-coupling reaction to produce intermediates **12a-12e**, which were then deprotected by TBAF to afford target compounds **B1–B5**.

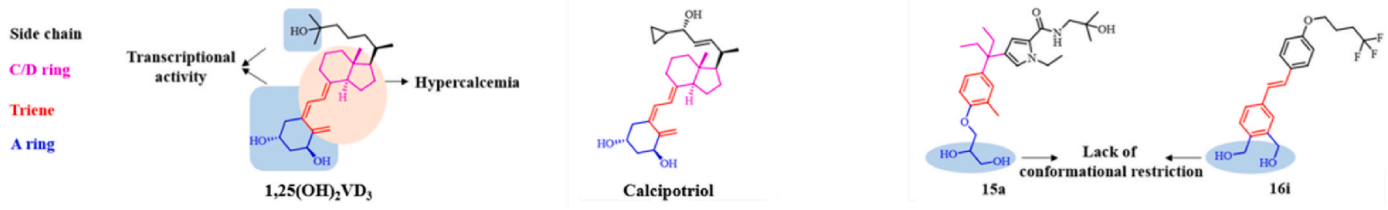

Fig. 1. Chemical structures of some secosteroidal and non-steroidal VDR ligands.

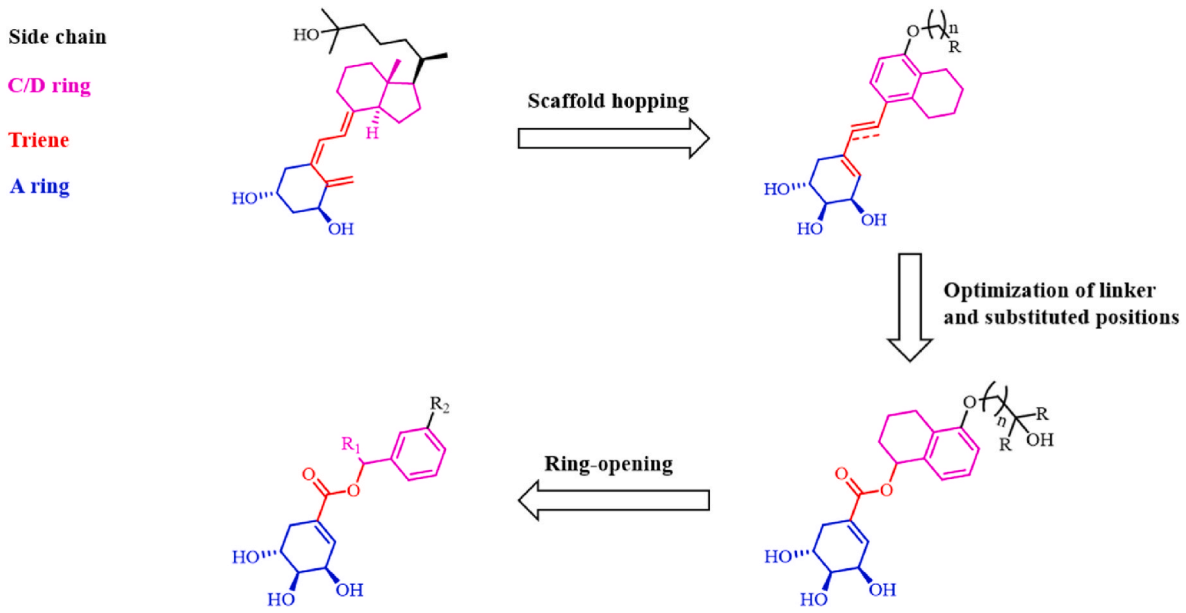

Fig. 2. Design concept of novel non-steroidal compounds.

The synthetic route of compounds **E1-E15** is shown in Scheme 3. Intermediate **2** was hydrolyzed with lithium hydroxide to form intermediate **13**. Compounds **14a-14b** were subjected to nucleophilic substitution reactions or Mitsunobu reactions to introduce different side chains, resulting in intermediates **17a-17k**. Intermediates **17a-17k** were reacted with sodium borohydride or Grignard reagents to yield intermediates **18a-18o**. Subsequently, these intermediates were reacted with intermediate **13** to obtain intermediates **19a-19o**, which were deprotected by *p*-toluenesulfonic acid to obtain the target compounds **E1-E15**. Reaction of intermediates **17a-17k** with sodium borohydride or Grignard reagents theoretically introduced new chiral centers, generating intermediates **18a-18i** and **18k-18o** as racemic mixtures. Consequently, the final compounds **E1-E8** and **E11-E15** are mixtures of diastereomers.

The synthetic route of compounds **E16-E17** is shown in Scheme 4. Compound **20** was subjected to a Miyaura borylation reaction to yield boronate ester **21**. This boronate ester was reacted with compound **22** through a Suzuki cross-coupling reaction to produce intermediate **23** which was reduced with sodium borohydride, subjected to a Grignard reaction, and then reacted with intermediate **13** to form intermediates **26a-26b**. Finally, the protection groups were removed using TBAF to obtain the target compounds **E16-E17**.

2.3. VDR binding affinity

To evaluate whether the synthesized compounds can bind to VDR, their relative VDR binding affinity was measured at a concentration of 1 μM using the fluorescence polarization assay. Calcipotriol, a known VDR agonist, was used as the positive control with its VDR binding affinity set at 100 %, while DMSO was used as the negative control with its VDR binding affinity set at 0 %. The relative VDR binding affinity for each test compound was calculated using the following formula: Relative VDR binding affinity (%) = ($mP_{DMSO} - mP_{Test\ Compound}$)/($mP_{DMSO} - mP_{Calcipotriene}$) × 100 %. As shown in Table 2, more than half of the compounds demonstrated higher VDR binding affinity compared to the previously reported non-steroidal VDR agonists **15a** and **16i**. Notably, compounds **A11**, **E11**, **E12**, and **E15** exhibited relative VDR binding affinities exceeding 80 %.

For the A series of compounds, the effect of chain length on VDR affinity followed the order: 1 > 2>3 > 4. Consequently, we selected the chain length of 1 to further investigate the impact of terminal groups on VDR binding affinity. Among alcohol groups, the hydrophobicity and steric hindrance order were: phenyl > dimethyl > *tert*-butyl > diethyl. For ketone groups, the order was: *p*-*tert*-butylphenyl > *p*-isopropylphenyl > phenyl > *tert*-butyl. Generally, large hydrophobic ketone/alcohol groups were more conducive to VDR binding. In the B series, the influence of chain length on VDR affinity followed the order: 2 > 3>1. The C series data indicated that replacing the tetrahydronaphthalene fragment with an indole ring and changing the substituent position to a meta-disubstituted benzene ring enhanced VDR binding. Comparing the B series with A and C series compounds, it was evident that compounds with trans double bonds as linkers had better VDR affinity than those with triple bonds. For compounds **E1-E9**, the chain length impact on VDR affinity was: 3 > 4>2, and the effect of terminal tertiary alcohol alkyl groups was: methyl > ethyl > n-propyl > allyl > n-butyl. For compounds **E10-E17**, the effect of benzyl alkyl groups on VDR affinity was: methyl > ethyl > n-propyl > n-butyl > hydrogen.

2.4. VDR agonistic activity

To further elucidate the VDR agonistic properties of the synthesized compounds, we initially assessed their capacity to upregulate the downstream VDR target gene *CYP24A1* [34] in the LX-2 cell line at a concentration of 0.5 μM, employing quantitative real-time polymerase chain reaction (qPCR) [35]. Furthermore, the transcriptional activity of the compounds at 0.5 μM was examined in HEK293 cells utilizing a dual-luciferase reporter assay. In this assay, calcipotriol was used as the positive control, while DMSO served as the negative control. The pGL4.27-SPP × 3-Luc reporter plasmid acted as the VDRE-activated reporter, and pRL-TK was used to normalize luciferase expression as an internal reference. The expression of VDR was increased using pENTER-CMV-hVDR, and RXRα, the VDR heterodimer partner, was expressed with pENTER-CMV-hRXRα [24]. As shown in Fig. 3, over one-third of the compounds significantly activated transcription of downstream VDR genes compared to the negative control, indicating effective VDR agonistic activity. Specifically, **A9**, **C2**, **E5**, **E15**, and **E17** significantly promoted *CYP24A1* expression in the qPCR assay.

Despite the differences observed between the two evaluation methods, there were some common trends in the transcriptional activity of the test compounds. For the A series compounds, the bulky ketone substituents were the most effective, followed by bulky alcohol

Table 1
Chemical structures of designed compounds.

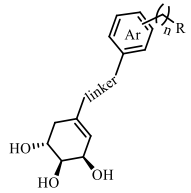

A1-A13, B1-B5, C1-C2

Compd.	linker	Ar	n	R	Compd.	linker	Ar	n	R
A1			1		**A11**			1	
A2			2		**A12**			1	
A3			3		**A13**			1	
A4			4		**B1**			2	
A5			1		**B2**			3	
A6			1		**B3**			3	
A7			1		**B4**			4	
A8			1		**B5**			4	
A9			1		**C1**			3	
A10			1		**C2**			3	

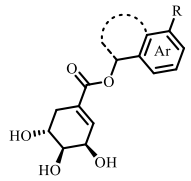

E1-E17

Compd.	Ar	R	Compd.	Ar	R
E1		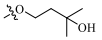	**E10**		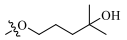
E2		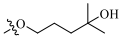	**E11**		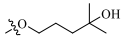
E3		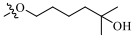	**E12**		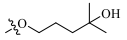
E4		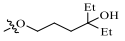	**E13**		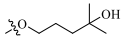
E5		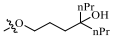	**E14**		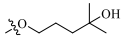
E6		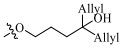	**E15**		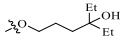
E7		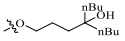	**E16**		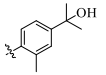
E8		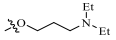	**E17**		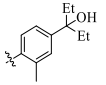
E9		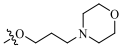			

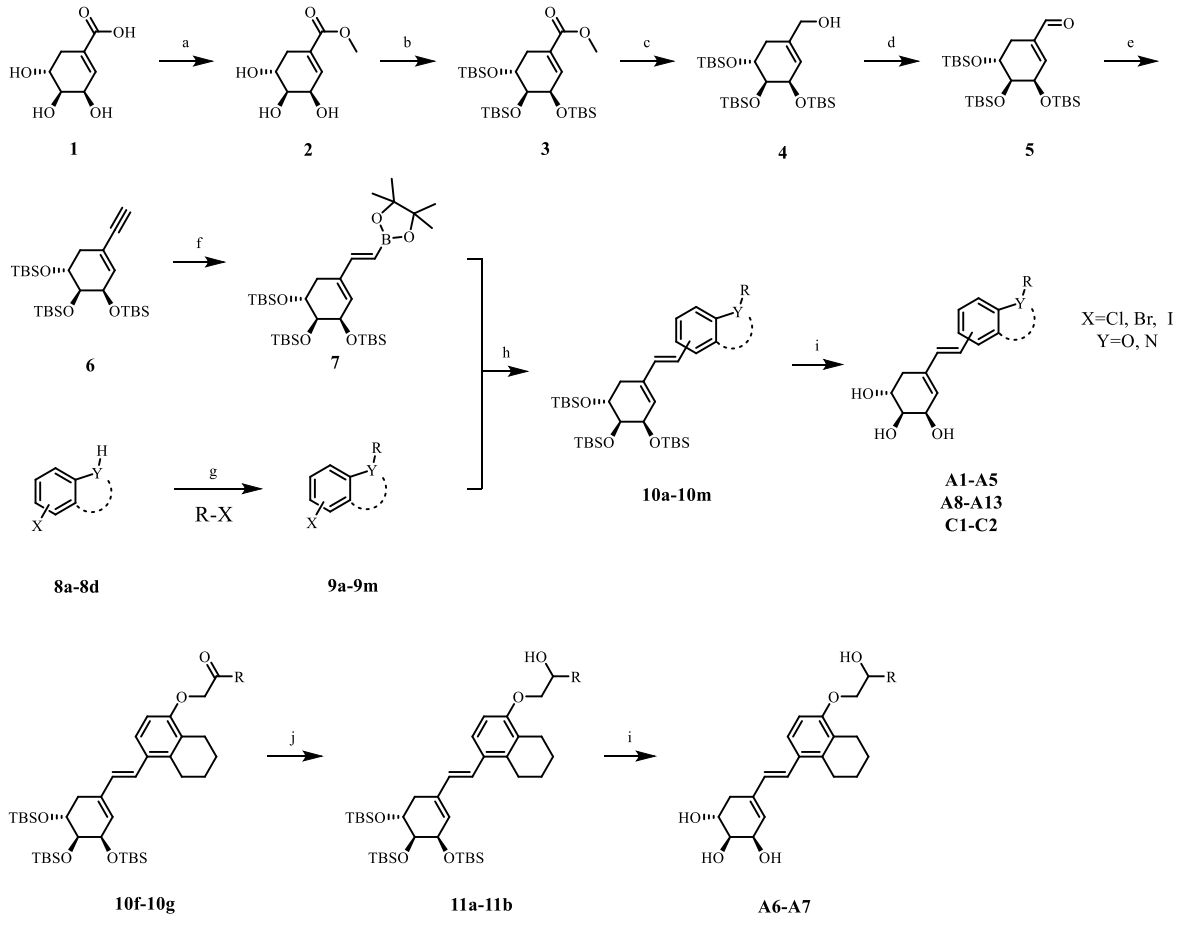

Scheme 1. Synthesis of target compounds **A1-A13** and compounds **C1–C2**. Reagents and conditions: (a) $SOCl_2$, MeOH, 70 °C; (b) TBSCl, imidazole, DMAP, DMF, 60 °C; (c) DIBAL-H, THF, 0 °C; (d) MnO_2, DCM, rt; (e) $TMSCHN_2$, nBuLi, THF, −78 °C; (f) B_2pin_2, CuCl, tBuOK, PPh_3, MeOH, THF, rt; (g) RX, NaH, KI, DMF, rt; (h) Pd(dppf)Cl_2, Cs_2CO_3, DMF/H_2O, 80 °C; (i) TBAF, THF, rt; (j) $NaBH_4$, THF/MeOH, 0 °C.

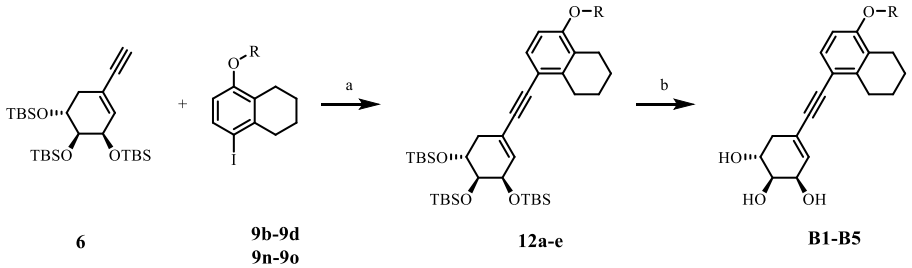

Scheme 2. Synthesis of target compounds **B1–B5**. Reagents and conditions: (a) Pd(dppf)Cl_2, CuI, Et_3N, 70 °C; (b) TBAF, THF, rt.

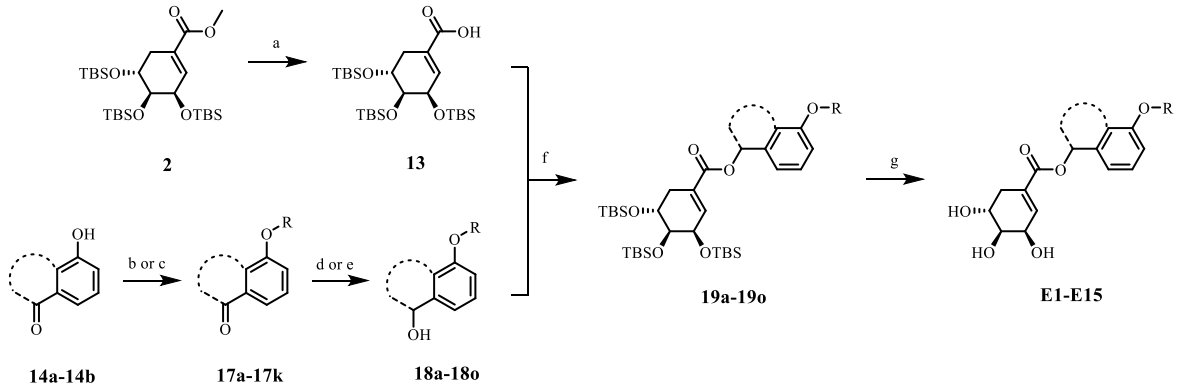

Scheme 3. Synthesis of target compounds **E1-E15**. Reagents and conditions: (a) LiOH, THF/H_2O, 50 °C; (b) RBr, K_2CO_3, KI, DMF, 45 °C; (c) ROH, DEAD, PPh_3, THF, rt; (d) $NaBH_4$, MeOH, 0 °C; (e) RMgBr, THF, 0 °C; (f) EDCI, DMAP, DMF, rt; (g) TsOH, MeOH, rt.

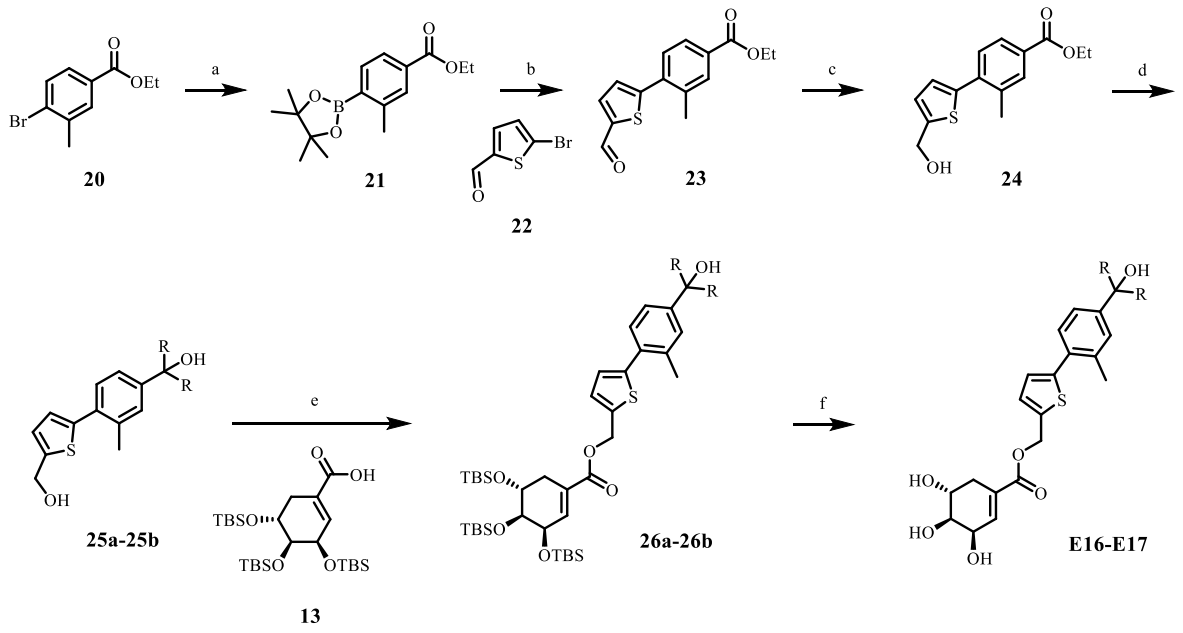

Scheme 4. Synthesis of target compounds **E16-E17**. Reagents and conditions: (a) B_2pin_2, $Pd(dppf)Cl_2$, AcOK, dioxane, 80 °C; (b) $Pd(dppf)Cl_2$, K_2CO_3, dioxane/H_2O, 80 °C; (c) $NaBH_4$, MeOH, 0 °C; (d) RMgBr, THF, 0 °C; (e) EDCI, DMAP, DMF, rt; (f) TBAF, THF, rt.

substituents, while the hydrophilic amide substituents did not exhibit transcriptional activity in either assay. For the E series compounds, those that showed transcriptional activation in the qPCR assay, such as **E5**, **E15**, and **E17**, also demonstrated significant transactivation ability in the dual-luciferase reporter assay. These overall trends were consistent with the binding affinities of most compounds, indicating that VDR binding affinity is generally a prerequisite for transcriptional activity. However, for a few compounds showing discrepancies, further mechanistic studies are needed.

2.5. Effect on the expression levels of α-SMA and collagen-I in LX-2 cell

Based on the results of VDR binding affinity and VDR agonistic activity evaluations, nine representative compounds were selected for in vitro antifibrotic activity assessment. The overexpression of collagen I and α-SMA, which are markers of hepatic fibrosis, is regarded as the primary characteristic of hepatic stellate cells (HSCs) activation. LX-2 cells were treated with different compounds at a concentration of 0.5 μM in the presence of 5 ng/mL TGF-β1 for 24 h [36]. The expression levels of *ACTA2* and *COL1A1* genes were measured using qPCR (Fig. 4A). And the protein levels of α-SMA and Collagen I were determined using Western blot analysis (Fig. 4B and Fig. S1).

Both qPCR and Western blot results demonstrated that the compounds with strong VDR binding affinity and agonistic activity, such as **A9**, **E5**, **E12**, **E13**, **E15**, and **E17**, could inhibit HSC activation to varying degrees. Among these, **E12**, **E13**, **E15** and **E17** exhibited a more potent inhibitory effect than previously reported non-steroidal agonists **15a** and **16i**. In contrast, compounds like **A7** and **E9**, which had VDR binding affinity but lacked VDR agonistic activity, showed minimal inhibitory effects on the expression of these proteins and showed expression levels of α-SMA and collagen I similar to or higher than those of the control, highlighting the need for further investigation into these discrepancies. These findings indicate that the VDR agonistic activity of the compounds is generally essential for their in vitro antifibrotic activity.

2.6. Compound E15 inhibited activation of LX-2 cells through VDR

To validate that the compound mediates its biological activity via VDR, we employed small interfering RNA (siRNA) to knock down VDR expression in LX2 cells. Following this, the LX2 cells were exposed to calcipotriol, **E15**, or **15a** at a concentration of 0.5 μM, in the presence of 5 ng/mL TGF-β1, for a duration of 24 h. As illustrated in Fig. 5, the absence of VDR abrogated the **E15**-induced suppression of collagen I and α-SMA expression, with calcipotriol and **15a** demonstrating similar effects. These results suggest that the compound **E15** exerts its inhibitory effects on HSC activation through its interaction with VDR.

2.7. Anti-fibrotic effect of E15 in CCl_4-induced hepatic fibrosis mice

Based on the results of in vitro activity assays, compound **E15**, which exhibited the most potent VDR agonistic and in vitro anti-fibrotic properties, was selected for subsequent in vivo activity evaluation. To preliminarily assess the anti-fibrotic effects of this compound, a hepatic fibrosis model was induced in C57BL/6 mice through intraperitoneal

Table 2
Relative VDR binding affinity of Synthetized compounds at 1 μM.

Compd.	VDR binding affinity (%)[a]	Compd.	VDR binding affinity (%)[a]	Compd.	VDR binding affinity (%)[a]
A1	72	**B2**	15	**E9**	50
A2	55	**B3**	-[b]	**E10**	49
A3	43	**B4**	50	**E11**	85
A4	21	**B5**	49	**E12**	84
A5	61	**C1**	71	**E13**	77
A6	50	**C2**	64	**E14**	50
A7	77	**E1**	45	**E15**	84
A8	68	**E2**	69	**E16**	71
A9	72	**E3**	65	**E17**	60
A10	76	**E4**	68	[c]DMSO	0
A11	88	**E5**	77	**15a**	57
A12	56	**E6**	51	**16i**	51
A13	45	**E7**	34	[d]Calcipotriol	100
B1	56	**E8**	64		

[a] Results were expressed as the mean relative VDR binding affinity of three experiments.
[b] No binding.
[c] DMSO was used as the negative control.
[d] Calcipotriol was used as the positive control.

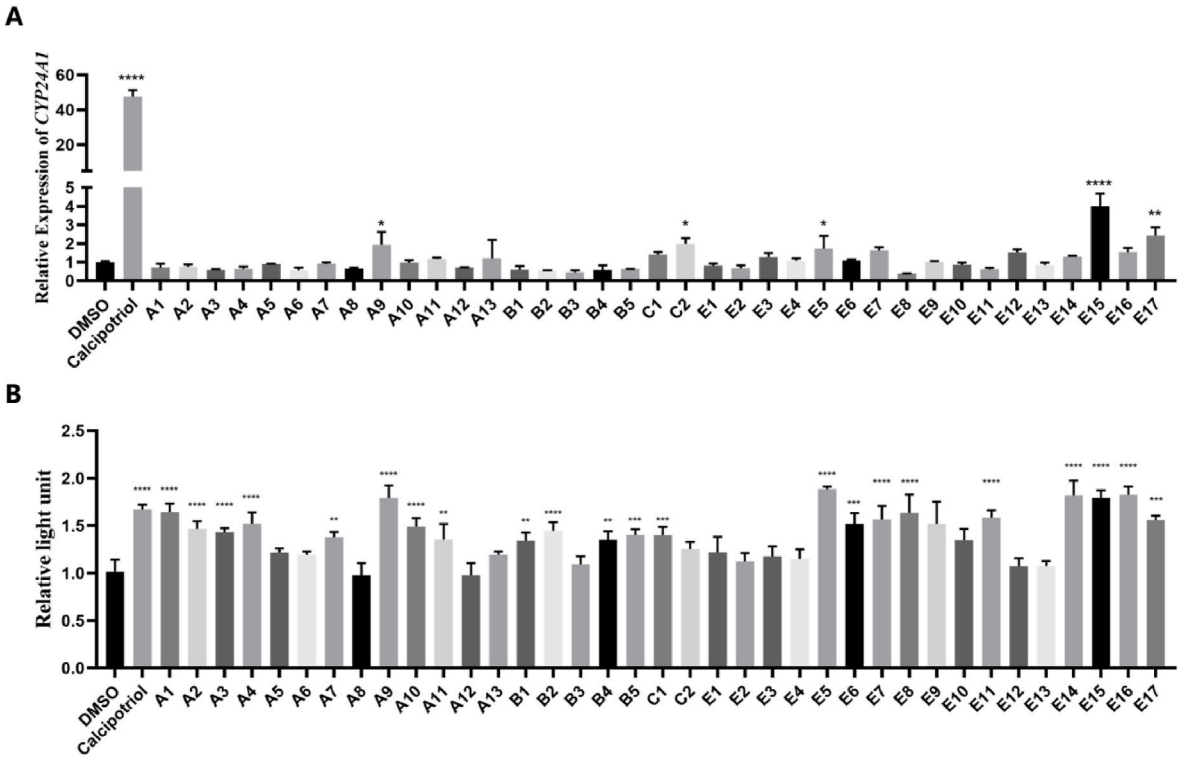

Fig. 3. (A)The relative expression of *CYP24A1* in LX-2 cells was detected by qPCR after treatment with different compounds at 0.5 μM, with calcipotriol as positive control and DMSO as negative control; (B) The VDR transactivation activity was detected in HEK293 cells using dual luciferase reporter genes after treatment with different compounds at 0.5 μM, with calcipotriol as positive control and DMSO as negative control (mean ± SD; *$P < 0.05$ vs DMSO, **$P < 0.01$ vs DMSO, ***$P < 0.001$ vs DMSO, ****$P < 0.0001$ vs DMSO).

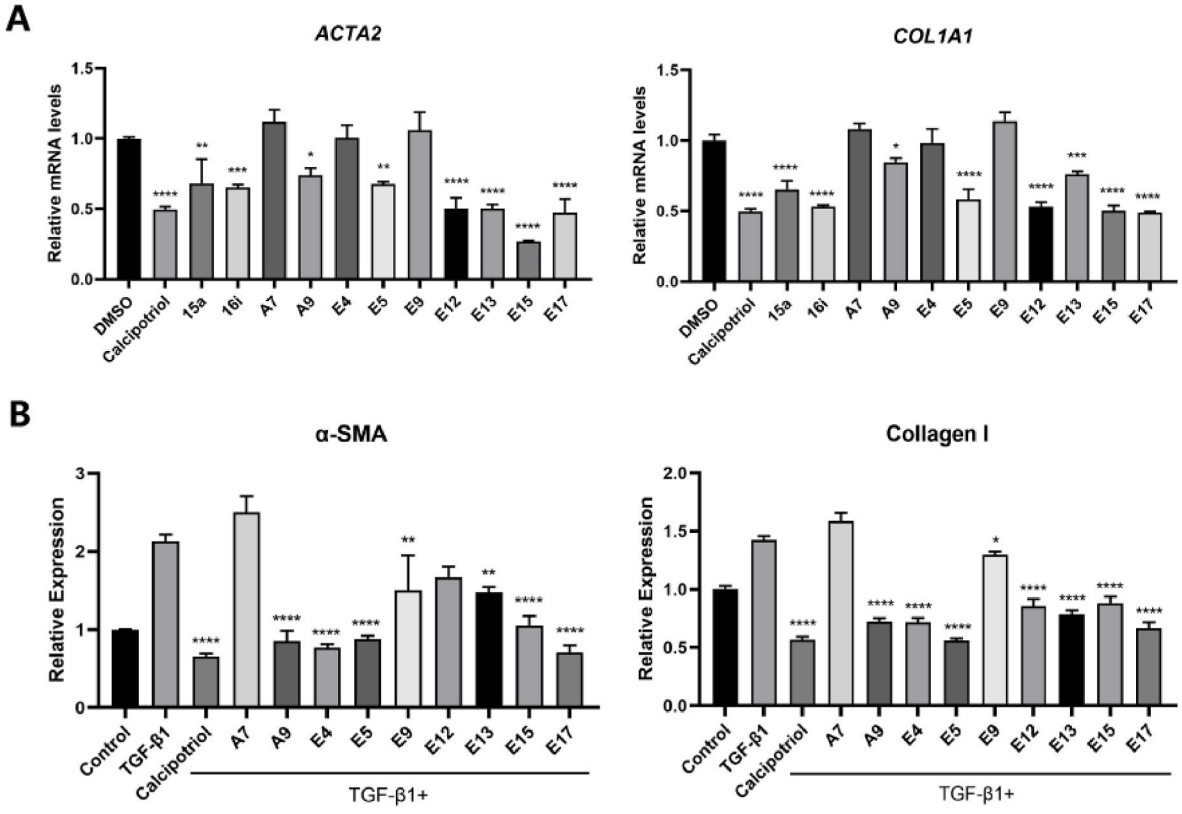

Fig. 4. (A) Relative expression of *ACTA2* and *COL1A1* in LX-2 cells was determined by qPCR, after treatment with different compounds at 0.5 μM, with calcipotriol, **15a** and **16i** as positive controls and DMSO as negative control (mean ± SD; *$P < 0.05$ vs DMSO, **$P < 0.01$ vs DMSO, ***$P < 0.001$ vs DMSO, ****$P < 0.0001$ vs DMSO). (B) Relative expression of collagen I and α-SMA proteins, normalized to the expression of β-actin protein (mean ± SD; *$P < 0.05$ vs TGF-β1, **$P < 0.01$ vs TGF-β1, ***$P < 0.001$ vs TGF-β1, ****$P < 0.0001$ vs TGF-β1).

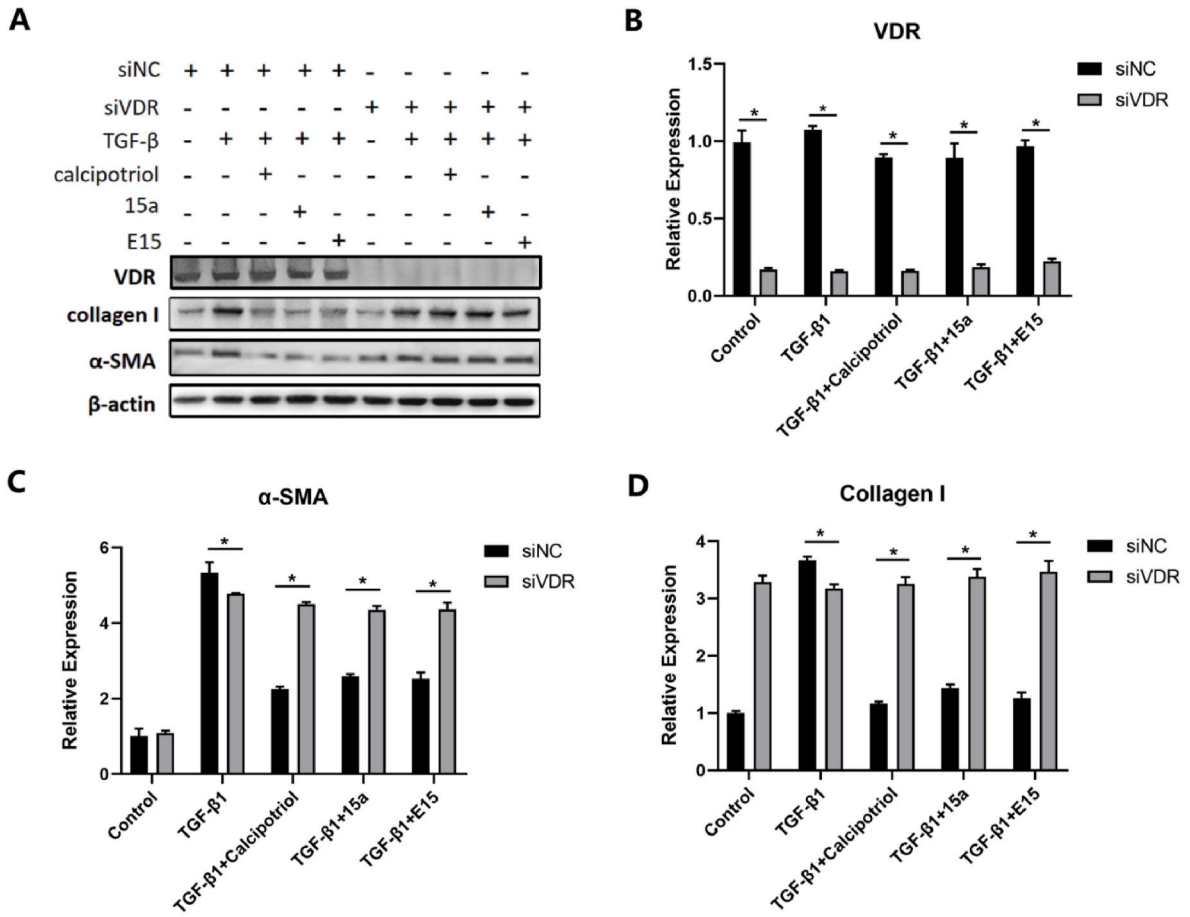

Fig. 5. Compound **E15** inhibited LX-2 activation via VDR. (A) VDR-specific (siVDR) or negative control (siNC) siRNA-transfected LX-2 cells were treated with **E15** (100 nM), TGF-β1 (1 ng/mL) or TGF-β1 plus **E15** for 24 h. The expression of VDR, α-SMA, and collagen I in LX-2 cells were tested by Western blot. The representative gel electrophoresis bands are shown. (B–D) Expression levels of VDR, α-SMA, and collagen I were normalized to the expression of β-actin. (mean ± SD; $^*P < 0.05$).

administration of CCl_4 over a four-week period. Commencing in the third week, the mice received daily oral gavage treatments for two weeks with either 100 μg/kg Calcipotriol, 500 μg/kg compound **15a**, or 500 μg/kg **E15**. At the end of the fourth week, mice were sacrificed, and blood and liver samples were collected for biochemical and histological analysis.

As shown in Fig. 6A, qPCR analysis demonstrated a significant inhibition of the expression levels of *Fn*, *Ctgf*, and *Timp-1*, which are implicated in the synthesis and degradation of the extracellular matrix (ECM) [37–39], were significantly inhibited in the livers of mice treated with compound **E15**. This contrasts with the up-regulation observed in the CCl_4 group. H&E and Masson's Trichrome staining revealed that **E15** effectively reduced hepatic lesions and collagen deposition (Fig. 6B and C). Furthermore, immunofluorescence staining indicated elevated levels of α-SMA in the CCl_4 group, suggesting HSC activation and liver fibrosis. In contrast, **E15** treatment suppressed this activation, achieving effects comparable to those of the positive control, calcipotriol (Fig. 6D). Inflammation often occurs during the process of liver fibrosis, the ELISA analysis demonstrated a decrease in the pro-inflammatory cytokine IL-1β and an increase in the anti-inflammatory cytokine IL-10 following **E15** treatment. (Fig. 6E–F). These findings suggest that **E15** effectively modulates inflammatory cytokine levels in the damaged liver, thereby mitigating the progression of liver fibrosis. Furthermore, **E15** treatment resulted in reduced levels of AST, ALT, and TBA, indicative of enhanced liver health (Fig. 6G). Notably, **E15** did not lead to an elevation in serum calcium levels compared to Calcipotriol (Fig. 6H), highlighting the distinct advantage of non-steroidal VDR agonists such as **E15** for long-term management of liver fibrosis.

2.8. Molecular docking study

To gain further insight into the interaction between **E15** and VDR, molecular docking was performed with two diastereomers of **E15**, S,R,S,R- and R,R,S,R-configurations, docked into the ligand-binding pocket of hVDR (PDB ID: 7QBB). The docking results (Fig. 7) revealed that the cyclohexene triol moiety of **E15** successfully mimicked the functional roles of the 1α and 3β hydroxyl groups of the A-ring in secosteroidal compounds, forming hydrogen bonds with key amino acids Tyr-143, Ser-237, Arg-274, and Ser-278 in the VDR ligand-binding domain (LBD). Additionally, the 2-hydroxyl group in the cyclohexene triol fragment formed an extra hydrogen bond with Ser-237, while the tertiary alcohol on the side chain formed a hydrogen bond with His-305. For.

S,R,S,R-configuration, the ethyl group at the benzyl position engaged in hydrophobic interactions with the crucial amino acid Trp-286 [40]. In contrast, for the R,R,S,R-configuration, these interactions were mediated by the phenyl ring interacting with Trp-286. The docking scores for the two diastereomers are −15.882 and −15.845, respectively, reflecting the strong binding affinity of **E15** for VDR. The superimposition of **E15** with 1α,25-$(OH)_2$-D_3 showed good overlap, successfully mimicking some features of 1α,25-$(OH)_2$-D_3.

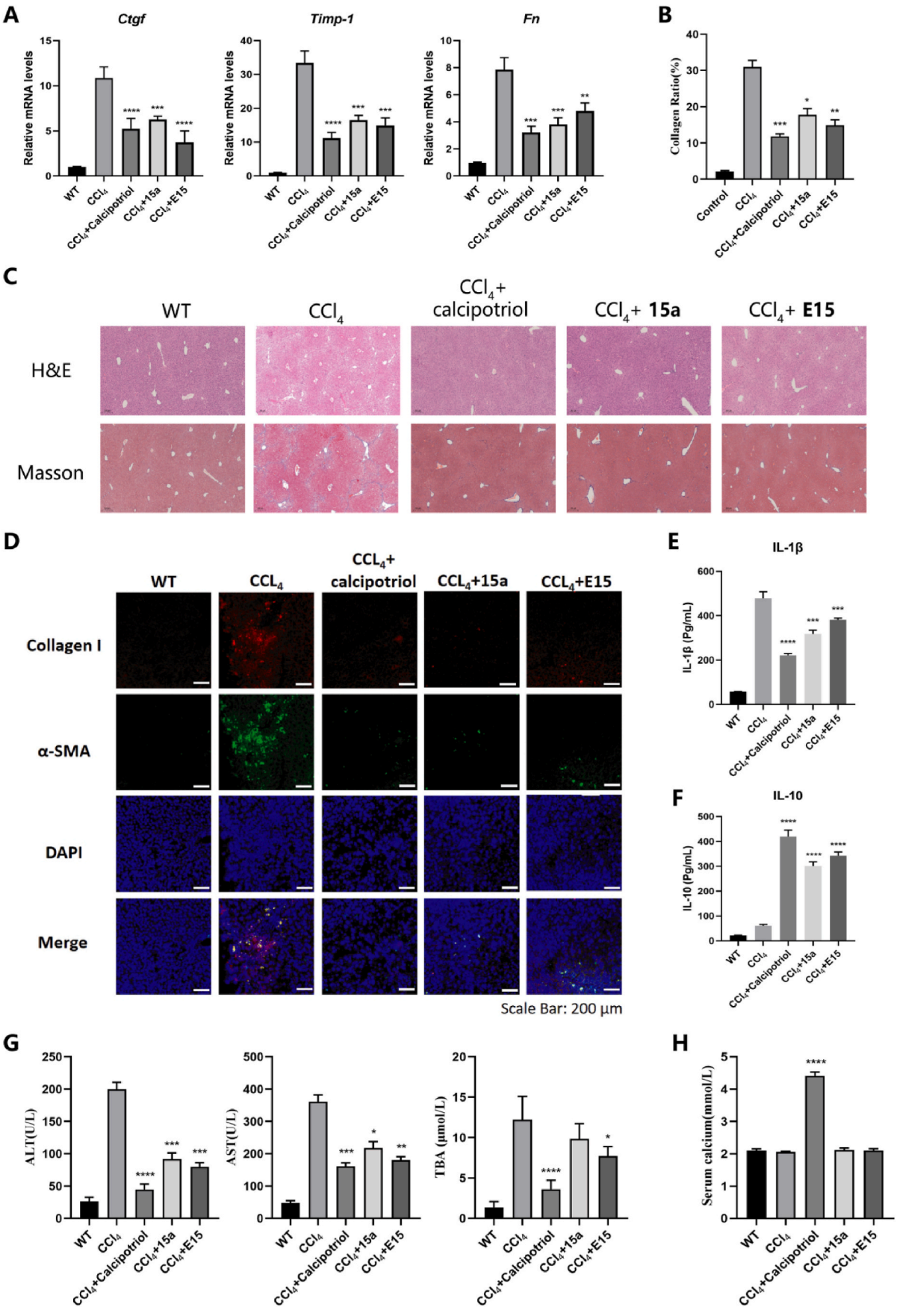

(caption on next page)

Fig. 6. In vivo therapeutic effect of compound **E15** on CCl_4-induced hepatic fibrosis mice. (A) Expression levels of *Fn*, *Ctgf*, and *Timp-1* were measured by qPCR (mean ± SD; *$P < 0.05$ vs CCl_4 group, **$P < 0.01$ vs CCl_4 group, ***$P < 0.001$ vs CCl_4 group, ****$P < 0.0001$ vs CCl_4 group). (B) The collagen ratio displayed by Masson's Trichrome staining. (C) CCl_4-induced hepatic fibrosis lesions were examined by H&E staining (× 100), and the collagen deposition was determined by Masson's Trichrome staining (× 100). (D) The expression of HSC activation markers, α-SMA and Collagen I were examined by immunofluorescence staining. (E) The expression level of IL-1β was measured by ELISA (mean ± SD; ***$P < 0.001$ vs CCl_4 group, ****$P < 0.0001$ vs CCl_4 group). (F) The expression level of IL-10 was measured by ELISA (mean ± SD, ****$P < 0.0001$ vs CCl_4 group). (G) Serum levels of ALT, AST, and TBA were determined (mean ± SD; *$P < 0.05$ vs CCl_4 group, **$P < 0.01$ vs CCl_4 group, ***$P < 0.001$ vs CCl_4 group, ****$P < 0.0001$ vs CCl_4 group). (H) Serum calcium concentration was determined by a calcium assay kit (mean ± SD; ****$P < 0.0001$ vs Control group).

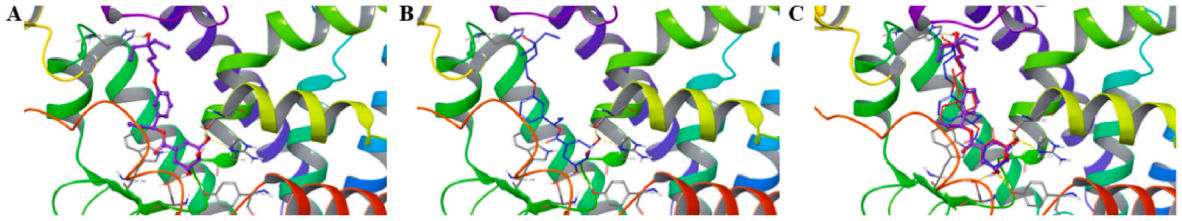

Fig. 7. Predicted binding model of **E15-(S, R, S, R)** (A) and **E15-(R, R, S, R)** (B). The VDR-LBD of PDB reference 7QBB was used in the molecular-docking analysis performed with Schrodinger 2018. (C) Superposition of **E15** and calcipotriol. Compound **E15-(S, R, S, R)** is depicted in purple, compound **E15-(R, R, S, R)** is depicted in blue and calcipotriol is in red. (For interpretation of the references to color in this figure legend, the reader is referred to the Web version of this article.)

3. Conclusion

In summary, a total of 37 compounds featuring novel scaffolds were designed and synthesized utilizing the principles of scaffold hopping, and their structure-activity relationships (SAR) were comprehensively analyzed. Of these compounds, more than one-third exhibited substantial binding affinity to the VDR and functioned as VDR agonists. Notably, compound **E15** displayed the highest VDR agonistic activity and demonstrated promising in vitro efficacy against HSC activation. Furthermore, in vivo studies of compound **E15** indicated significant antifibrotic effects in a CCl_4-induced mouse model of liver fibrosis. Histological analysis revealed that the administration of **E15** resulted in a reduction of lesions, inflammatory cell infiltration, and collagen deposition. Biochemical assays demonstrated that **E15** effectively decreased the levels of hepatic fibrosis markers and serum liver function indices. Notably, **E15** ameliorated liver fibrosis without significantly affecting serum calcium levels, a side effect associated with the positive control, calcipotriol. It is worth noting that some compounds in this study, including **A6-7**, **E1-8**, and **E11**–**15**, are mixtures of diastereomers, which require further resolution to investigate the properties of individual stereoisomers. Meanwhile, as the E-series compounds contain ester bonds, there may be concerns about their metabolic stability in vivo, which requires further confirmation and optimization in future studies.

4. Experimental section

4.1. Chemistry

All used materials and solvents were obtained from commercial venders and used without further purification. Reactions were monitored by thin layer chromatography (TLC), and the related compounds were separated by column chromatography on silica gel (100–200 mesh). Mass spectra (MS) were recorded on a QSTAR XL Hybrid MS/MS mass spectrometer. ^{1}H NMR and ^{13}C NMR spectra were recorded on Bruker AV-300 spectrometer with $CDCl_3$, CD_3OD or DMSO-d_6 as solvents. The chemical shifts were signified in ppm (δ) relative to the internal standard tetramethylsilane (TMS), and coupling constants were signified in hertz (Hz). The purity of the test compounds was analyzed by HPLC, and that for all compounds was ≥95 %.

4.1.1. Synthesis of methyl (3R,4S,5R)-3,4,5-trihydroxycyclohex-1-ene-1-carboxylate (2)

To a suspension of shikimic acid (50 g, 287.11 mmol) in methanol (300 mL), thionyl chloride (9.4 mL, 0.13 mol) was added at room temperature. Then, the resulting mixture was refluxed at 70 °C for 6 h and monitored by TLC. After the reaction was completed, the mixture was cooled to room temperature and was then concentrated under reduced pressure to give a brown oil, which was recrystallized with ethyl acetate to give compound 2 as a white solid. Yield: 84 %.

4.1.2. Synthesis of methyl (3R,4S,5R)-3,4,5-tris((tert-butyldimethylsilyl)oxy)cyclohex-1-ene-1-carboxylate (3)

To a solution of compound **2** (45.1 g, 239.67 mmol), imidazole (57.11 g, 838.83 mmol) and DMAP (5.86 g, 47.93 mmol) in DMF (150 mL) was added TBSCl (119.2 g, 790.9 mmol) at room temperature. The reaction was stirred at 60 °C for 12 h and was monitored by TLC. After the reaction was completed, the mixture was cooled to room temperature, quenched with brine (50 mL) and extracted with ethyl acetate (2 × 150 mL). The organic extracts were washed with brine (3 × 150 mL), dried over Na_2SO_4, and concentrated under reduced pressure. The crude product was purified by column chromatography with petroleum ether/ethyl acetate (50/1, v/v) as the eluent to give compound **3** as a white solid. Yield: 90 %.

4.1.3. Synthesis of ((3R,4S,5R)-3,4,5-tris((tert-butyldimethylsilyl)oxy)cyclohex-1-en-1-yl)methanol (4)

To a solution of compound **3** (50 g, 94.17 mmol) in THF (200 mL) was added DIBAL-H (1.5 M solution in toluene, 138 mL, 207.17 mmol) dropwise under argon atmosphere at 0 °C. The reaction was stirred at 0 °C for 2 h and was monitored by TLC. After the reaction was completed, the mixture was quenched with saturated aqueous potassium sodium tartrate solution (150 mL), diluted with water (100 mL) and extracted with ethyl acetate (3 × 150 mL). The organic extracts were dried over Na_2SO_4 and concentrated under reduced pressure. The crude product was purified by column chromatography using petroleum ether/ethyl acetate (12/1, v/v) as the eluent to afford compound **4** as a white solid. Yield: 95 %.

4.1.4. Synthesis of (3R,4S,5R)-3,4,5-tris((tert-butyldimethylsilyl)oxy)cyclohex-1-ene-1-carbaldehyde (5)

To a solution of compound **4** (44.95 g, 89.37 mmol) in DCM (200 mL) was added active manganese dioxide (77.7 g, 893.71 mmol). The reaction was stirred at room temperature for 24 h and was monitored by

TLC. After the reaction was completed, the mixture was then filtered through a pad of Celite, and the filter cake was washed with DCM (100 mL). The filtrate was concentrated under reduced pressure and purified by column chromatography eluting with petroleum ether/ethyl acetate (50/1, v/v) to obtain compound **5** as a white solid. Yield: 91 %.

4.1.5. Synthesis of (3R,4S,5R) −3,4,5-tris ((tert-butyldimethylsilyl)oxy) -1-ethynyl cyclohexene (6)

To a solution of $TMSCHN_2$ (2 M solution in hexane, 37.5 mL, 75 mmol) in THF (150 mL) was added n-BuLi (2.5 M solution in toluene, 30 mL, 75 mmol) dropwise under argon atmosphere at −78 °C. After 30 min, compound **5** (25 g, 49.91 mmol) in THF (20 mL) was added dropwise at −78 °C. After 1 h the mixture was stirred for 8 h at room temperature and was monitored by TLC. After the reaction was completed, the mixture was quenched with saturated aqueous NH_4Cl solution (50 mL), diluted with water (100 mL) and extracted with ethyl acetate (3 × 100 mL). The organic extracts were dried over Na_2SO_4 and concentrated under reduced pressure. The crude product was purified by column chromatography with petroleum ether/DCM (20/1, v/v) as the eluent to afford compound **6** as a yellow oil. Yield: 56 %.

4.1.6. Synthesis of (1R,2S,3R) −1,2,3-tri ((tert-butyldimethylsilyl)oxy) -5- ((E) -2- (4,4,5,5-tetramethyl-1,3,2-dioxaborolan-2-yl) vinyl) cyclohex-4-ene (7)

An oven-dried Schlenk flask was charged CuCl (0.20 g, 2.01 mmol), tBuOK (0.23 g, 2.01 mmol), PPh_3 (1.05 g, 4.02 mmol) and THF (80 mL). The suspension was stirred at room temperature for 0.5 h under argon atmosphere and then, B_2pin_2 (5.62 g, 22.13 mmol) in THF (20 mL) were added. The reaction mixture was stirred for another 0.5 h and compound **6** (10g, 20.12 mmol) was added, followed by MeOH (1.63 ml, 40.25 mmol). The resulting mixture was stirred at room temperature for 8 h and was monitored by TLC. After the reaction was completed, the mixture was quenched with saturated aqueous NH_4Cl solution (50 mL) and extracted with ethyl acetate (3 × 50 mL). The organic extracts were dried over Na_2SO_4 and concentrated under reduced pressure. The crude product was purified by column chromatography using petroleum ether/DCM (10/1, v/v) as the eluent to afford compound **7** as a yellow paste. Yield: 72 %.

4.1.7. Synthesis of 4-iodo-5,6,7,8-tetrahydronaphthalen-1-ol (8a)

To a solution of 5,6,7,8-tetrahydronaphthalen-1-ol (25 g, 168.69 mmol) in MeCN (250 mL) was added trifluoroacetic acid (2.59 mL, 33.74 mmol) at room temperature. After 5 min, NIS (13.28 g × 3, 177.12 mmol) was added in three portions. The reaction was stirred at room temperature for 6 h and was monitored by TLC. After the reaction was completed, the mixture was quenched with saturated aqueous sodium thiosulphate solution (50 mL), diluted with water (100 mL) and extracted with ethyl acetate (3 × 100 mL). The organic extracts were dried over Na_2SO_4 and concentrated under reduced pressure. The crude product was purified by column chromatography eluting petroleum ether/ethyl acetate (15/1, v/v) to obtain compound 8a as a yellow solid. Yield: 68 %.

4.1.8. General procedure 1: synthesis of compounds 9a-9q

To a solution of one of compounds **9a-9o** (10 mmol) in DMF (30 mL) was added NaH (12 mmol) at room temperature. After 30 min, alkyl halide (15 mmol) and KI (2 mmol) were added. The reaction was stirred at room temperature for 2 h and was monitored by TLC. After the reaction was completed, the mixture was quenched with brine (30 mL) and extracted with ethyl acetate (2 × 30 mL). The organic extracts were washed with brine (3 × 50 mL), dried over Na_2SO_4, and concentrated under reduced pressure. The crude products were purified by column chromatography eluting with 5–20 % ethyl acetate in petroleum ether.

4.1.8.1. 1-((4-iodo-5,6,7,8-tetrahydronaphthalen-1-yl)oxy)-2-methylpropan-2-ol (9a). A yellow oil. Yield: 61 %.

4.1.8.2. 4-((4-iodo-5,6,7,8-tetrahydronaphthalen-1-yl)oxy)-2-methylbutan-2-ol (9b). A yellow oil. Yield: 78 %.

4.1.8.3. 5-((4-iodo-5,6,7,8-tetrahydronaphthalen-1-yl)oxy)-2-methylpentan-2-ol (9c). A yellow oil. Yield: 34 %.

4.1.8.4. 6-((4-iodo-5,6,7,8-tetrahydronaphthalen-1-yl)oxy)-2-methylhexan-2-ol (9d). A yellow oil. Yield: 75 %.

4.1.8.5. 3-(((4-iodo-5,6,7,8-tetrahydronaphthalen-1-yl)oxy)methyl)pentan-3-ol (9e). A yellow oil. Yield: 58 %.

4.1.8.6. 1-((4-iodo-5,6,7,8-tetrahydronaphthalen-1-yl)oxy)-3,3-dimethylbutan-2-one (9f). A white solid. Yield: 73 %.

4.1.8.7. 2-((4-iodo-5,6,7,8-tetrahydronaphthalen-1-yl)oxy)-1-phenylethan-1-one (9g). A yellow solid. Yield: 65 %.

4.1.8.8. 2-((4-iodo-5,6,7,8-tetrahydronaphthalen-1-yl)oxy)-1-(4-isopropylphenyl)ethan-1-one (9h). A white solid. Yield: 62 %.

4.1.8.9. 1-(4-(tert-butyl)phenyl)-2-((4-iodo-5,6,7,8-tetrahydronaphthalen-1-yl)oxy)ethan-1-one (9i). A white solid. Yield: 68 %.

4.1.8.10. N,N-diethyl-2-((4-iodo-5,6,7,8-tetrahydronaphthalen-1-yl)oxy) acetamide (9j). A yellow oil. Yield: 80 %.

4.1.8.11. 2-((4-iodo-5,6,7,8-tetrahydronaphthalen-1-yl)oxy)-1-morpholinoethan-1-one (9k). A yellow oil. Yield: 78 %.

4.1.8.12. 5-(4-bromo-1H-indol-1-yl)-2-methylpentan-2-ol (9l). A yellow oil. Yield: 23 %.

4.1.8.13. 6-(4-bromo-1H-indol-1-yl)-3-ethylhexan-3-ol (9 m). A yellow oil. Yield: 20 %.

4.1.8.14. 3-Ethyl-6-((4-iodo-5,6,7,8-tetrahydronaphthalen-1-yl)oxy) hexan-3-ol (9n). A yellow oil. Yield: 37 %.

4.1.8.15. 3-Ethyl-7-((4-iodo-5,6,7,8-tetrahydronaphthalen-1-yl)oxy)heptan-3-ol (9o). A yellow oil. Yield: 69 %.

4.1.9. General procedure 2: synthesis of compounds 10a-10 m

To a suspension of one of compounds **9a-9m** (2 mmol), compound **7** (2.3 mmol), Cs_2CO_3 (5 mmol) and $Pd(dppf)Cl_2$ (0.1 mmol) in DMF (10 mL) was added water (0.5 mL) at room temperature. The suspension was stirred at 80 °C for 4 h under argon atmosphere and was monitored by TLC. After the reaction was completed, the mixture was cooled to room temperature and was then filtered through a pad of Celite. The filter cake was washed with ethyl acetate (50 mL), and the filtrate was washed with brine (3 × 30 mL), dried over Na_2SO_4, and concentrated under reduced pressure. The crude products were purified by column chromatography eluting with 2–15 % ethyl acetate in petroleum ether.

4.1.9.1. 2-Methyl-1-((4-((E)-2-((3R,4S,5R)-3,4,5-tris((tert-butyldimethylsilyl)oxy)cyclohex-1-en-1-yl)vinyl)-5,6,7,8-tetrahydronaphthalen-1-yl) oxy)propan-2-ol (10a). A yellow oil. Yield: 62 %.

4.1.9.2. 2-Methyl-4-((4-((E)-2-((3R,4S,5R)-3,4,5-tris((tert-butyldimethylsilyl)oxy)cyclohex-1-en-1-yl)vinyl)-5,6,7,8-tetrahydronaphthalen-1-yl) oxy)butan-2-ol (10b). A yellow oil. Yield: 70 %.

4.1.9.3. 2-Methyl-5-((4-((E)-2-((3R,4S,5R)-3,4,5-tris((tert-butyldimethylsilyl)oxy)cyclohex-1-en-1-yl)vinyl)-5,6,7,8-tetrahydronaphthalen-1-yl)oxy)pentan-2-ol (10c). A yellow oil. Yield: 65 %.

4.1.9.4. 2-Methyl-6-((4-((E)-2-((3R,4S,5R)-3,4,5-tris((tert-butyldimethylsilyl)oxy)cyclohex-1-en-1-yl)vinyl)-5,6,7,8-tetrahydronaphthalen-1-yl)oxy)hexan-2-ol (10d). A yellow oil. Yield: 60 %.

4.1.9.5. 3-(((4-((E)-2-((3R,4S,5R)-3,4,5-tris((tert-butyldimethylsilyl)oxy)cyclohex-1-en-1-yl)vinyl)-5,6,7,8-tetrahydronaphthalen-1-yl)oxy)methyl)pentan-3-ol (10e). A yellow oil. Yield: 54 %.

4.1.9.6. 3,3-Dimethyl-1-((4-((E)-2-((3R,4S,5R)-3,4,5-tris((tert-butyldimethylsilyl)oxy)cyclohex-1-en-1-yl)vinyl)-5,6,7,8-tetrahydronaphthalen-1-yl)oxy)butan-2-one (10f). A yellow oil. Yield: 58 %.

4.1.9.7. 1-Phenyl-2-((4-((E)-2-((3R,4S,5R)-3,4,5-tris((tert-butyldimethylsilyl)oxy)cyclohex-1-en-1-yl)vinyl)-5,6,7,8-tetrahydronaphthalen-1-yl)oxy)ethan-1-one (10g). A yellow oil. Yield: 67 %.

4.1.9.8. 1-(4-isopropylphenyl)-2-((4-((E)-2-((3R,4S,5R)-3,4,5-tris((tert-butyldimethylsilyl)oxy)cyclohex-1-en-1-yl)vinyl)-5,6,7,8-tetrahydronaphthalen-1-yl)oxy)ethan-1-one (10h). A yellow oil. Yield: 75 %.

4.1.9.9. 1-(4-(tert-butyl)phenyl)-2-((4-((E)-2-((3R,4S,5R)-3,4,5-tris((tert-butyldimethylsilyl)oxy)cyclohex-1-en-1-yl)vinyl)-5,6,7,8-tetrahydronaphthalen-1-yl)oxy)ethan-1-one (10i). A yellow oil. Yield: 60 %.

4.1.9.10. N,N-diethyl-2-((4-((E)-2-((3R,4S,5R)-3,4,5-tris((tert-butyldimethylsilyl)oxy)cyclohex-1-en-1-yl)vinyl)-5,6,7,8-tetrahydronaphthalen-1-yl)oxy)acetamide (10j). A yellow oil. Yield: 78 %.

4.1.9.11. 1-Morpholino-2-((4-((E)-2-((3R,4S,5R)-3,4,5-tris((tert-butyldimethylsilyl)oxy)cyclohex-1-en-1-yl)vinyl)-5,6,7,8-tetrahydronaphthalen-1-yl)oxy)ethan-1-one (10k). A yellow oil. Yield: 64 %.

4.1.9.12. 2-Methyl-5-(4-((E)-2-((3R,4S,5R)-3,4,5-tris((tert-butyldimethylsilyl)oxy)cyclohex-1-en-1-yl)vinyl)-1H-indol-1-yl)pentan-2-ol (10l). A yellow oil. Yield: 56 %.

4.1.9.13. 3-Ethyl-6-(4-((E)-2-((3R,4S,5R)-3,4,5-tris((tert-butyldimethylsilyl)oxy)cyclohex-1-en-1-yl)vinyl)-1H-indol-1-yl)hexan-3-ol (10 m). A yellow oil. Yield: 52 %.

4.1.10. General procedure 3: synthesis of compounds 11a-11b

To a solution of compound **10f** or **10g** (0.6 mmol) in THF (5 mL) was added MeOH (1 mL) and $NaBH_4$ (0.2 mmol) at 0 °C. The reaction was stirred at room temperature for 1 h and was monitored by TLC. After the reaction was completed, the mixture was quenched with brine (10 mL) and extracted with ethyl acetate (3 × 30 mL). The organic extracts were dried over Na_2SO_4, and concentrated under reduced pressure. The crude products were used in the next step without further purification.

4.1.10.1. 3,3-Dimethyl-1-((4-((E)-2-((3R,4S,5R)-3,4,5-tris((tert-butyldimethylsilyl)oxy)cyclohex-1-en-1-yl)vinyl)-5,6,7,8-tetrahydronaphthalen-1-yl)oxy)butan-2-ol (11a). A colorless oil. Yield: 86 %.

4.1.10.2. 1-Phenyl-2-((4-((E)-2-((3R,4S,5R)-3,4,5-tris((tert-butyldimethylsilyl)oxy)cyclohex-1-en-1-yl)vinyl)-5,6,7,8-tetrahydronaphthalen-1-yl)oxy)ethan-1-ol (11b). A yellow oil. Yield: 89 %.

4.1.11. General procedure 4: synthesis of target compounds A1-A13 and C1–C2

To a solution of one of compounds **10a-10m** and **11a-11b** (0.3 mmol) in THF (3 mL) was added TBAF (1 mL, 1 M in THF) dropwise at room temperature. The reaction was stirred at room temperature for 6 h and was monitored by TLC. After the reaction was finished, the mixture was quenched with saturated aqueous NH_4Cl solution (5 mL) and extracted with ethyl acetate (3 × 15 mL). The organic extracts were washed with brine (3 × 20 mL) dried over Na_2SO_4, and concentrated under reduced pressure. The crude products were purified by column chromatography.

4.1.11.1. (1R,2S,3R)-5-((E)-2-(4-(2-hydroxy-2-methylpropoxy)-5,6,7,8-tetrahydronaphthalen-1-yl)vinyl)cyclohex-4-ene-1,2,3-triol (A1). A yellow paste. Yield: 31 %.

4.1.11.2. (1R,2S,3R)-5-((E)-2-(4-(3-hydroxy-3-methylbutoxy)-5,6,7,8-tetrahydronaphthalen-1-yl)vinyl)cyclohex-4-ene-1,2,3-triol (A2). A light yellow solid. Yield: 49 %.

4.1.11.3. (1R,2S,3R)-5-((E)-2-(4-((4-hydroxy-4-methylpentyl)oxy)-5,6,7,8-tetrahydronaphthalen-1-yl)vinyl)cyclohex-4-ene-1,2,3-triol (A3). A yellow solid. Yield: 55 %.

4.1.11.4. (1R,2S,3R)-5-((E)-2-(4-((5-hydroxy-5-methylhexyl)oxy)-5,6,7,8-tetrahydronaphthalen-1-yl)vinyl)cyclohex-4-ene-1,2,3-triol (A4). A yellow oil. Yield: 51 %.

4.1.11.5. (1R,2S,3R)-5-((E)-2-(4-(2-ethyl-2-hydroxybutoxy)-5,6,7,8-tetrahydronaphthalen-1-yl)vinyl)cyclohex-4-ene-1,2,3-triol (A5). A yellow paste. Yield: 45 %.

4.1.11.6. (1R,2S,3R)-5-((E)-2-(4-(2-hydroxy-3,3-dimethylbutoxy)-5,6,7,8-tetrahydronaphthalen-1-yl)vinyl)cyclohex-4-ene-1,2,3-triol (A6). A white solid. Yield: 63 %.

4.1.11.7. (1R,2S,3R)-5-((E)-2-(4-(2-hydroxy-2-phenylethoxy)-5,6,7,8-tetrahydronaphthalen-1-yl)vinyl)cyclohex-4-ene-1,2,3-triol (A7). A yellow solid. Yield: 57 %.

4.1.11.8. 3,3-Dimethyl-1-((4-((E)-2-((3R,4S,5R)-3,4,5-trihydroxycyclohex-1-en-1-yl)vinyl)-5,6,7,8-tetrahydronaphthalen-1-yl)oxy)butan-2-one (A8). A yellow solid. Yield: 57 %.

4.1.11.9. 1-Phenyl-2-((4-((E)-2-((3R,4S,5R)-3,4,5-trihydroxycyclohex-1-en-1-yl)vinyl)-5,6,7,8-tetrahydronaphthalen-1-yl)oxy)ethan-1-one (A9). A yellow solid. Yield: 42 %.

4.1.11.10. 1-(4-isopropylphenyl)-2-((4-((E)-2-((3R,4S,5R)-3,4,5-trihydroxycyclohex-1-en-1-yl)vinyl)-5,6,7,8-tetrahydronaphthalen-1-yl)oxy)ethan-1-one (A10). A white solid. Yield: 55 %.

4.1.11.11. 1-(4-(tert-butyl)phenyl)-2-((4-((E)-2-((3R,4S,5R)-3,4,5-trihydroxycyclohex-1-en-1-yl)vinyl)-5,6,7,8-tetrahydronaphthalen-1-yl)oxy)ethan-1-one (A11). A yellow oil. Yield: 55 %.

4.1.11.12. N,N-diethyl-2-((4-((E)-2-((3R,4S,5R)-3,4,5-trihydroxycyclohex-1-en-1-yl)vinyl)-5,6,7,8-tetrahydronaphthalen-1-yl)oxy)acetamide (A12). A yellow solid. Yield: 75 %.

4.1.11.13. 1-Morpholino-2-((4-((E)-2-((3R,4S,5R)-3,4,5-trihydroxycyclohex-1-en-1-yl)vinyl)-5,6,7,8-tetrahydronaphthalen-1-yl)oxy)ethan-1-one (A13). A yellow solid. Yield: 72 %.

4.1.11.14. (1R,2S,3R)-5-((E)-2-(1-(4-hydroxy-4-methylpentyl)-1H-indol-4-yl)vinyl)cyclohex-4-ene-1,2,3-triol (C1). A yellow oil. Yield: 46 %.

4.1.11.15. (1R,2S,3R)-5-((E)-2-(1-(4-ethyl-4-hydroxyhexyl)-1H-indol-4-yl)vinyl)cyclohex-4-ene-1,2,3-triol (C2). A yellow paste. Yield: 55 %.

4.1.12. General procedure 5: synthesis of compounds 12a-12e

An oven-dried Schlenk flask was charged one of compounds **9b-9d** or **9n-9o** (1 mmol), compound **6** (1.1 mmol), CuI (0.1 mmol), $Pd(dppf)Cl_2$ (0.05 mmol) and Et_3N (5 mL). The solution was stirred at 70 °C for 1 h under argon atmosphere and was monitored by TLC. After the reaction was completed, the mixture was cooled to room temperature and was then filtered through a pad of Celite. The filter cake was washed with ethyl acetate (30 mL), and the filtrate was washed with brine (3 × 20 mL), dried over Na_2SO_4, and concentrated under reduced pressure. The crude products were purified by column chromatography eluting with 8 % ethyl acetate in petroleum ether.

4.1.12.1. 2-Methyl-4-((4-(((3R,4S,5R)-3,4,5-tris((tert-butyldimethylsilyl)oxy)cyclohex-1-en-1-yl)ethynyl)-5,6,7,8-tetrahydronaphthalen-1-yl)oxy)butan-2-ol (12a). A yellow oil. Yield: 78 %.

4.1.12.2. 2-Methyl-5-((4-(((3R,4S,5R)-3,4,5-tris((tert-butyldimethylsilyl)oxy)cyclohex-1-en-1-yl)ethynyl)-5,6,7,8-tetrahydronaphthalen-1-yl)oxy)pentan-2-ol (12b). A yellow oil. Yield: 75 %.

4.1.12.3. 3-Ethyl-6-((4-(((3R,4S,5R)-3,4,5-tris((tert-butyldimethylsilyl)oxy)cyclohex-1-en-1-yl)ethynyl)-5,6,7,8-tetrahydronaphthalen-1-yl)oxy)hexan-3-ol (12c). A yellow oil. Yield: 72 %.

4.1.12.4. 2-Methyl-6-((4-(((3R,4S,5R)-3,4,5-tris((tert-butyldimethylsilyl)oxy)cyclohex-1-en-1-yl)ethynyl)-5,6,7,8-tetrahydronaphthalen-1-yl)oxy)hexan-2-ol (12d). A yellow oil. Yield: 69 %.

4.1.12.5. 3-Ethyl-7-((4-(((3R,4S,5R)-3,4,5-tris((tert-butyldimethylsilyl)oxy)cyclohex-1-en-1-yl)ethynyl)-5,6,7,8-tetrahydronaphthalen-1-yl)oxy)heptan-3-ol (12e). A yellow oil. Yield: 77 %.

4.1.13. Synthesis of target compounds B1–B5

The target compounds **B1–B5** are synthesized using general procedure 4.

4.1.13.1. (1R,2S,3R)-5-((4-(3-hydroxy-3-methylbutoxy)-5,6,7,8-tetrahydronaphthalen-1-yl)ethynyl)cyclohex-4-ene-1,2,3-triol (B1). A light yellow solid. Yield: 63 %.

4.1.13.2. (1R,2S,3R)-5-((4-((4-hydroxy-4-methylpentyl)oxy)-5,6,7,8-tetrahydronaphthalen-1-yl)ethynyl)cyclohex-4-ene-1,2,3-triol (B2). A yellow paste. Yield: 70 %.

4.1.13.3. (1R,2S,3R)-5-((4-((4-ethyl-4-hydroxyhexyl)oxy)-5,6,7,8-tetrahydronaphthalen-1-yl)ethynyl)cyclohex-4-ene-1,2,3-triol (B3). A yellow paste. Yield: 68 %.

4.1.13.4. (1R,2S,3R)-5-((4-((5-hydroxy-5-methylhexyl)oxy)-5,6,7,8-tetrahydronaphthalen-1-yl)ethynyl)cyclohex-4-ene-1,2,3-triol (B4). A yellow paste. Yield: 52 %.

4.1.13.5. (1R,2S,3R)-5-((4-((5-ethyl-5-hydroxyheptyl)oxy)-5,6,7,8-tetrahydronaphthalen-1-yl)ethynyl)cyclohex-4-ene-1,2,3-triol (B5). A yellow oil. Yield: 50 %.

4.1.14. Synthesis of (3R,4S,5R)-3,4,5-tris((tert-butyldimethylsilyl)oxy)cyclohex-1-ene-1-carboxylic acid (13)

To a solution of compound **3** (50 g, 94.17 mmol) in THF (200 mL) was added water (40 mL) and lithium hydroxide (6.77 g, 282.50 mmol). The reaction was stirred at 50 °C for 6 h and was monitored by TLC. After the reaction was completed, the mixture was cooled to room temperature and the pH was adjusted to 5 using 4 M hydrochloric acid. The mixture was extracted with ethyl acetate (3 × 100 mL), and the organic extracts were dried over Na_2SO_4, and concentrated under reduced pressure. The crude product was purified by column chromatography with petroleum ether/ethyl acetate (10/1, v/v) as the eluent to obtain compound 13 as a white solid. Yield: 83 %.

4.1.15. General procedure 6: synthesis of compounds 17a-17g and 17j-17k

To a solution of compound **14a** or **14b** (5 mmol) in DMF (10 mL) was added K_2CO_3 (10 mmol), alkyl bromide (7.5 mmol) and KI (1 mmol). The mixture was stirred at 45 °C for 8 h and was monitored by TLC. After the reaction was completed, the mixture was cooled to room temperature and was then diluted with ethyl acetate (30 mL), washed with brine (3 × 30 mL), dried over Na_2SO_4, and concentrated under reduced pressure. The crude products were purified by column chromatography eluting 15%–20 % ethyl acetate in petroleum ether.

4.1.15.1. 5-(3-hydroxy-3-methylbutoxy)-3,4-dihydronaphthalen-1(2H)-one (17a). A yellow oil. Yield: 53 %.

4.1.15.2. 5-((4-hydroxy-4-methylpentyl)oxy)-3,4-dihydronaphthalen-1(2H)-one (17b). A yellow oil. Yield: 43 %.

4.1.15.3. 5-((5-hydroxy-5-methylhexyl)oxy)-3,4-dihydronaphthalen-1(2H)-one (17c). A yellow oil. Yield: 62 %.

4.1.15.4. 5-((4-ethyl-4-hydroxyhexyl)oxy)-3,4-dihydronaphthalen-1(2H)-one (17d). A yellow oil. Yield: 47 %.

4.1.15.5. 5-((4-hydroxy-4-propylheptyl)oxy)-3,4-dihydronaphthalen-1(2H)-one (17e). A yellow oil. Yield: 55 %.

4.1.15.6. 5-((4-allyl-4-hydroxyhept-6-en-1-yl)oxy)-3,4-dihydronaphthalen-1(2H)-one (17f). A yellow oil. Yield: 42 %.

4.1.15.7. 5-((4-butyl-4-hydroxyoctyl)oxy)-3,4-dihydronaphthalen-1(2H)-one (17g). A yellow oil. Yield: 51 %.

4.1.15.8. 3-((4-hydroxy-4-methylpentyl)oxy)benzaldehyde (17j). A yellow oil. Yield: 60 %.

4.1.15.9. 3-((4-ethyl-4-hydroxyhexyl)oxy)benzaldehyde (17k). A yellow oil. Yield: 64 %.

4.1.16. General procedure 7: synthesis of compounds 17h-17i

To a solution of compound **14a** (0.5g, 3.08 mmol), amino alcohols (3.39 mmol) and PPh_3 (4.62 mmol) in THF (10 mL) was added DEAD (4.62 mmol) dropwise at 0 °C under argon atmosphere. The reaction was then stirred at room temperature for 8 h and was monitored by TLC. After the reaction was completed, the mixture was concentrated under reduced pressure. The crude products were purified by column chromatography eluting 2%–5% MeOH in DCM.

4.1.16.1. 5-(3-(diethylamino)propoxy)-3,4-dihydronaphthalen-1(2H)-one (17h). A yellow oil. Yield: 49 %.

4.1.16.2. 5-(3-morpholinopropoxy)-3,4-dihydronaphthalen-1(2H)-one (17i). A yellow oil. Yield: 65 %.

4.1.17. General procedure 8: synthesis of compounds 18a-18j

To a solution of one of the compounds **17a-17j** (1 mmol) in MeOH (5 mL) was added $NaBH_4$ (0.3 mmol) at 0 °C. The reaction was stirred at room temperature for 1 h and was monitored by TLC. After the reaction was completed, the mixture was quenched with brine (10 mL) and extracted with ethyl acetate (3 × 20 mL). The organic extracts were

dried over Na_2SO_4, and concentrated under reduced pressure. The crude products were used in the next step without purification.

4.1.17.1. 5-(3-hydroxy-3-methylbutoxy)-1,2,3,4-tetrahydronaphthalen-1-ol (18a). A yellow oil. Yield: 92 %.

4.1.17.2. 5-((4-hydroxy-4-methylpentyl)oxy)-1,2,3,4-tetrahydronaphthalen-1-ol (18b). A yellow oil. Yield: 90 %.

4.1.17.3. 5-((5-hydroxy-5-methylhexyl)oxy)-1,2,3,4-tetrahydronaphthalen-1-ol (18c). A yellow oil. Yield: 89 %.

4.1.17.4. 5-((4-ethyl-4-hydroxyhexyl)oxy)-1,2,3,4-tetrahydronaphthalen-1-ol (18d). A yellow oil. Yield: 96 %.

4.1.17.5. 5-((4-hydroxy-4-propylheptyl)oxy)-1,2,3,4-tetrahydronaphthalen-1-ol (18e). A yellow oil. Yield: 95 %.

4.1.17.6. 5-((4-allyl-4-hydroxyhept-6-en-1-yl)oxy)-1,2,3,4-tetrahydronaphthalen-1-ol (18f). A yellow oil. Yield: 85 %.

4.1.17.7. 5-((4-butyl-4-hydroxyoctyl)oxy)-1,2,3,4-tetrahydronaphthalen-1-ol (18g). A yellow oil. Yield: 98 %

4.1.17.8. 5-(3-(diethylamino)propoxy)-1,2,3,4-tetrahydronaphthalen-1-ol (18h). A yellow oil. Yield: 87 %.

4.1.17.9. 5-(3-morpholinopropoxy)-1,2,3,4-tetrahydronaphthalen-1-ol (18i). A yellow oil. Yield: 90 %.

4.1.17.10. 5-(3-(hydroxymethyl)phenoxy)-2-methylpentan-2-ol (18j). A yellow oil. Yield: 91 %.

4.1.18. General procedure 9: synthesis of compounds 18k-18o

To a solution of compound **17j** or **17k** (0.3 mmol) in THF was added RMgBr (0.66 mmol) dropwise at 0 °C under argon atmosphere. The mixture was then stirred at room temperature for 30 min and was monitored by TLC. After the reaction was completed, the mixture was quenched with saturated aqueous NH_4Cl solution (20 mL) and extracted with ethyl acetate (3 × 30 mL). The organic extracts were dried over Na_2SO_4, and concentrated under reduced pressure. The crude products were used in the next step without purification.

4.1.18.1. 5-(3-(1-hydroxyethyl)phenoxy)-2-methylpentan-2-ol (18k). A yellow oil. Yield: 84 %.

4.1.18.2. 5-(3-(1-hydroxypropyl)phenoxy)-2-methylpentan-2-ol (18l). A yellow oil. Yield: 82 %.

4.1.18.3. 5-(3-(1-hydroxybutyl)phenoxy)-2-methylpentan-2-ol (18 m). A yellow oil. Yield: 90 %.

4.1.18.4. 1-(3-((4-hydroxy-4-methylpentyl)oxy)phenyl)pentan-1-ol (18n). A yellow oil. Yield: 95 %.

4.1.18.5. 3-Ethyl-6-(3-(1-hydroxypropyl)phenoxy)hexan-3-ol (18o). A yellow oil. Yield: 91 %.

4.1.19. General procedure 10: synthesis of compounds 19a-19o

To a solution of one of compounds **18**–**18o** (0.2 mmol), compound **13** (0.22 mmol) and DMAP (0.24 mmol) in DMF (5 mL) was added EDCI (0.24 mmol). The reaction was stirred at room temperature for 12 h and was monitored by TLC. After the reaction was completed, the mixture was diluted with ethyl acetate (30 mL), washed with brine (3 × 30 mL), dried over Na_2SO_4, and concentrated under reduced pressure. The crude products were purified by column chromatography eluting 10 % ethyl acetate in petroleum ether or 2%–5% MeOH in DCM.

4.1.19.1. 5-(3-hydroxy-3-methylbutoxy)-1,2,3,4-tetrahydronaphthalen-1-yl (3R,4S,5R)-3,4,5-tris((tert-butyldimethylsilyl)oxy)cyclohex-1-ene-1-carboxylate (19a). A yellow oil. Yield: 75 %.

4.1.19.2. 5-((4-hydroxy-4-methylpentyl)oxy)-1,2,3,4-tetrahydronaphthalen-1-yl (3R,4S,5R)-3,4,5-tris((tert-butyldimethylsilyl)oxy)cyclohex-1-ene-1-carboxylate (19b). A yellow oil. Yield: 70 %.

4.1.19.3. 5-((5-hydroxy-5-methylhexyl)oxy)-1,2,3,4-tetrahydronaphthalen-1-yl (3R,4S,5R)-3,4,5-tris((tert-butyldimethylsilyl)oxy)cyclohex-1-ene-1-carboxylate (19c). A yellow oil. Yield: 80 %.

4.1.19.4. 5-((4-ethyl-4-hydroxyhexyl)oxy)-1,2,3,4-tetrahydronaphthalen-1-yl (3R,4S,5R)-3,4,5-tris((tert-butyldimethylsilyl)oxy)cyclohex-1-ene-1-carboxylate (19d). A colorless oil. Yield: 74 %.

4.1.19.5. 5-((4-hydroxy-4-propylheptyl)oxy)-1,2,3,4-tetrahydronaphthalen-1-yl (3R,4S,5R)-3,4,5-tris((tert-butyldimethylsilyl)oxy)cyclohex-1-ene-1-carboxylate (19e). A yellow oil. Yield: 85 %.

4.1.19.6. 5-((4-allyl-4-hydroxyhept-6-en-1-yl)oxy)-1,2,3,4-tetrahydronaphthalen-1-yl (3R,4S,5R)-3,4,5-tris((tert-butyldimethylsilyl)oxy) cyclohex-1-ene-1-carboxylate (19f). A yellow oil. Yield: 69 %.

4.1.19.7. 5-((4-butyl-4-hydroxyoctyl)oxy)-1,2,3,4-tetrahydronaphthalen-1-yl (3R,4S,5R)-3,4,5-tris((tert-butyldimethylsilyl)oxy)cyclohex-1-ene-1-carboxylate (19g). A colorless oil. Yield: 56 %.

4.1.19.8. 5-(3-(diethylamino)propoxy)-1,2,3,4-tetrahydronaphthalen-1-yl (3R,4S,5R)-3,4,5-tris((tert-butyldimethylsilyl)oxy)cyclohex-1-ene-1-carboxylate (19h). A yellow oil. Yield: 72 %.

4.1.19.9. 5-(3-morpholinopropoxy)-1,2,3,4-tetrahydronaphthalen-1-yl (3R,4S,5R)-3,4,5-tris((tert-butyldimethylsilyl)oxy)cyclohex-1-ene-1-carboxylate (19i). A yellow oil. Yield: 85 %.

4.1.19.10. 3-((4-hydroxy-4-methylpentyl)oxy)benzyl (3R,4S,5R)-3,4,5-tris((tert-butyldimethylsilyl)oxy)cyclohex-1-ene-1-carboxylate (19j). A yellow oil. Yield: 72 %.

4.1.19.11. 1-(3-((4-hydroxy-4-methylpentyl)oxy)phenyl)ethyl (3R,4S,5R)-3,4,5-tris((tert-butyldimethylsilyl)oxy)cyclohex-1-ene-1-carboxylate (19k). A yellow oil. Yield: 65 %.

4.1.19.12. 1-(3-((4-hydroxy-4-methylpentyl)oxy)phenyl)propyl (3R,4S,5R)-3,4,5-tris((tert-butyldimethylsilyl)oxy)cyclohex-1-ene-1-carboxylate (19l). A yellow oil. Yield: 77 %.

4.1.19.13. 1-(3-((4-hydroxy-4-methylpentyl)oxy)phenyl)butyl (3R,4S,5R)-3,4,5-tris((tert-butyldimethylsilyl)oxy)cyclohex-1-ene-1-carboxylate (19 m). A yellow oil. Yield: 69 %.

4.1.19.14. 1-(3-((4-hydroxy-4-methylpentyl)oxy)phenyl)pentyl (3R,4S,5R)-3,4,5-tris((tert-butyldimethylsilyl)oxy)cyclohex-1-ene-1-carboxylate (19n). A yellow oil. Yield: 58 %.

4.1.19.15. 1-(3-((4-ethyl-4-hydroxyhexyl)oxy)phenyl)propyl (3R,4S,5R)-3,4,5-tris((tert-butyldimethylsilyl)oxy)cyclohex-1-ene-1-carboxylate (19o). A yellow oil. Yield: 65 %.

4.1.20. General procedure 11: synthesis of target compounds E1-E15

To a solution of one of compounds **19a-19o** (0.3 mmol) in MeOH (5 mL) was added TsOH (0.1 mmol). The reaction was stirred at room temperature for 4 h and was monitored by TLC. After the reaction was completed, the reaction was quenched with saturated aqueous $NaHCO_3$ solution (1 mL) and extracted with ethyl acetate (3 × 20 mL). The organic extracts were dried over Na_2SO_4, and concentrated under reduced pressure. The crude products were purified by column chromatography.

4.1.20.1. 5-(3-hydroxy-3-methylbutoxy)-1,2,3,4-tetrahydronaphthalen-1-yl (3R,4S,5R)-3,4,5-trihydroxycyclohex-1-ene-1-carboxylate (E1). A white paste. Yield: 61 %.

4.1.20.2. 5-((4-hydroxy-4-methylpentyl)oxy)-1,2,3,4-tetrahydronaphthalen-1-yl (3R,4S,5R)-3,4,5-trihydroxycyclohex-1-ene-1-carboxylate (E2). A light yellow paste. Yield: 65 %.

4.1.20.3. 5-((5-hydroxy-5-methylhexyl)oxy)-1,2,3,4-tetrahydronaphthalen-1-yl (3R,4S,5R)-3,4,5-trihydroxycyclohex-1-ene-1-carboxylate (E3). A white paste. Yield: 56 %

4.1.20.4. 5-((4-ethyl-4-hydroxyhexyl)oxy)-1,2,3,4-tetrahydronaphthalen-1-yl (3R,4S,5R)-3,4,5-trihydroxycyclohex-1-ene-1-carboxylate (E4). A white paste. Yield: 70 %.

4.1.20.5. 5-((4-hydroxy-4-propylheptyl)oxy)-1,2,3,4-tetrahydronaphthalen-1-yl (3R,4S,5R)-3,4,5-trihydroxycyclohex-1-ene-1-carboxylate (E5). A white paste. Yield: 62 %.

4.1.20.6. 5-((4-allyl-4-hydroxyhept-6-en-1-yl)oxy)-1,2,3,4-tetrahydronaphthalen-1-yl (3R,4S,5R)-3,4,5-trihydroxycyclohex-1-ene-1-carboxylate (E6). A yellow paste. Yield: 54 %.

4.1.20.7. 5-((4-butyl-4-hydroxyoctyl)oxy)-1,2,3,4-tetrahydronaphthalen-1-yl (3R,4S,5R)-3,4,5-trihydroxycyclohex-1-ene-1-carboxylate (E7). A yellow paste. Yield: 50 %.

4.1.20.8. 5-(3-(diethylamino)propoxy)-1,2,3,4-tetrahydronaphthalen-1-yl (3R,4S,5R)-3,4,5-trihydroxycyclohex-1-ene-1-carboxylate (E8). A yellow oil. Yield: 45 %.

4.1.20.9. 5-(3-morpholinopropoxy)-1,2,3,4-tetrahydronaphthalen-1-yl (3R,4S,5R)-3,4,5-trihydroxycyclohex-1-ene-1-carboxylate (E9). A white paste. Yield: 60 %.

4.1.20.10. 3-((4-hydroxy-4-methylpentyl)oxy)benzyl (3R,4S,5R)-3,4,5-trihydroxycyclohex-1-ene-1-carboxylate (E10). A yellow paste. Yield: 68 %.

4.1.20.11. 1-(3-((4-hydroxy-4-methylpentyl)oxy)phenyl)ethyl (3R,4S,5R)-3,4,5-trihydroxycyclohex-1-ene-1-carboxylate (E11). A light yellow paste. Yield:71 %.

4.1.20.12. 1-(3-((4-hydroxy-4-methylpentyl)oxy)phenyl)propyl (3R,4S,5R)-3,4,5-trihydroxycyclohex-1-ene-1-carboxylate (E12). A light yellow oil. Yield: 65 %.

4.1.20.13. 1-(3-((4-hydroxy-4-methylpentyl)oxy)phenyl)butyl (3R,4S,5R)-3,4,5-trihydroxycyclohex-1-ene-1-carboxylate (E13). A white paste. Yield: 68 %.

4.1.20.14. 1-(3-((4-hydroxy-4-methylpentyl)oxy)phenyl)pentyl (3R,4S,5R)-3,4,5-trihydroxycyclohex-1-ene-1-carboxylate (E14). A colorless oil. Yield: 73 %.

4.1.20.15. 1-(3-((4-ethyl-4-hydroxyhexyl)oxy)phenyl)propyl (3R,4S,5R)-3,4,5-trihydroxycyclohex-1-ene-1-carboxylate (E15). A white paste. Yield: 77 %.

4.1.21. Synthesis of ethyl 4-(5-formylthiophen-2-yl)-3-methylbenzoate (23)

To a solution of compound **20** (2g, 8.23 mmol), B_2pin_2 (2.3g, 9.05 mmol) and $Pd(dppf)Cl_2$ (301 mg, 0.41 mmol) in anhydrous dioxane (50 mL) was added AcOK (1.61g, 16.45 mmol). The reaction was stirred at 80 °C under argon atmosphere for 12 h and was monitored by TLC. After complete conversion of the aryl bromide to the borate ester, the reaction was cooled to room temperature and then, compound **22** (1.37g, 7.41 mmol), K_2CO_3 (2.85g, 20.59 mmol), $Pd(dppf)Cl_2$ (120 mg, 0.16 mmol) and water (5 mL) were added in sequence. The resulting mixture was refluxed at 100 °C under argon atmosphere for 4 h and was monitored by TLC. After the reaction was finished, the mixture was cooled to room temperature and was then filtered through a pad of Celite. The filter cake was washed with ethyl acetate (100 mL), and the filtrate was washed with brine (3 × 30 mL), dried over Na_2SO_4, and concentrated under reduced pressure. The crude products were purified by column chromatography eluting with 6.5 % ethyl acetate in petroleum ether to afford compound **23** as a brown solid. Yield: 39 %.

4.1.22. Synthesis of ethyl 4-(5-(hydroxymethyl)thiophen-2-yl)-3-methylbenzoate (24)

The compound **24** was synthesized using general procedure 8. A light yellow oil. Yield: 92 %.

4.1.23. Synthesis of compound 25a-25b

The compounds **25a** and **25b** were synthesized according to general procedure 9.

4.1.23.1. 2-(4-(5-(hydroxymethyl)thiophen-2-yl)-3-methylphenyl)propan-2-ol (25a). A yellow oil. Yield: 78 %.

4.1.23.2. 3-(4-(5-(hydroxymethyl)thiophen-2-yl)-3-methylphenyl)pentan-3-ol (25b). A yellow oil. Yield: 72 %.

4.1.24. Synthesis of compounds 26a-26b

The compounds **26a** and **26b** were synthesized using general procedure 10.

4.1.24.1. (5-(4-(2-hydroxypropan-2-yl)-2-methylphenyl)thiophen-2-yl) methyl (3R,4S,5R)-3,4,5-tris((tert-butyldimethylsilyl)oxy)cyclohex-1-ene-1-carboxylate (26a). A yellow oil. Yield: 58 %.

4.1.24.2. (5-(4-(3-hydroxypentan-3-yl)-2-methylphenyl)thiophen-2-yl) methyl (3R,4S,5R)-3,4,5-tris((tert-butyldimethylsilyl)oxy)cyclohex-1-ene-1-carboxylate (26b). A yellow oil. Yield: 68 %.

4.1.25. Synthesis of target compounds E16-E17

The compounds **E16** and **E17** were synthesized using general procedure 4.

4.1.25.1. (5-(4-(2-hydroxypropan-2-yl)-2-methylphenyl)thiophen-2-yl) methyl (3R,4S,5R)-3,4,5-trihydroxycyclohex-1-ene-1-carboxylate (E16). A white paste. Yield: 65 %.

4.1.25.2. (5-(4-(3-hydroxypentan-3-yl)-2-methylphenyl)thiophen-2-yl) methyl (3R,4S,5R)-3,4,5-trihydroxycyclohex-1-ene-1-carboxylate (E17). A light yellow paste. Yield: 59 %.

4.2. VDR binding assay

The VDR binding affinity assay was conducted using the PolarScreen™ Vitamin D Receptor Competitor Assay, Red Kit (Thermo Fisher, Massachusetts, USA), which is designed to determine the IC_{50} values of compounds that bind to the full-length VDR. This assay measures the decrease in polarization value that occurs when the binding of VDR Full Length to the Fluormone™ Tracer is disrupted by the presence of a competitor compound. All test compounds were prepared in 1 % DMSO solution and evaluated for their binding affinity at a concentration of 1 μM, with each measurement performed in triplicate. Fluorescence polarization was measured using a BioTek Cytation 5 Multiscan Spectrum, equipped with a 535 nm excitation filter (25 nm bandwidth) and a 590 nm emission filter (20 nm bandwidth). The fluorescence polarization value of Calcipotriol was set as the standard at 100 %, and the relative binding affinity of each test compound was calculated using the following formula: $(mP_{DMSO} - mP_{Test\ compound})/(mP_{DMSO} - mP_{Calcipotriene}) \times 100$ %.

4.3. RNA extraction and quantitative real-time polymerase chain reaction (qPCR)

cDNA was generated from RNA extracts derived from cultured LX-2 cells or liver tissues using the HiScript II Q RT SuperMix for Q-PCR (+ gDNA wiper Mix) (Vazyme, Nanjing, China). β-actin (human) or β-actin (mouse) was used as an internal control. Q-PCR was performed using the Hieff® Q-PCR SYBR Green Master Mix (High Rox Plus) (Vazyme, Nanjing, China). The primer pairs of mRNA used are listed in Table S1.

4.4. Transcription assay

The luciferase activity assay was conducted using the Dual-Luciferase Reporter Assay System (Vazyme, Nanjing, China) following the manufacturer's guidelines. HEK293 cells at 50–60 % confluence were seeded in 48-well plates. For each well, the transfection mixture included 140 ng of TK-SPP × 3-Luci reporter plasmid, 20 ng of pCMX-Renilla, 30 ng of pENTER-CMV-hRXRα, and 100 ng of pCMX-VDR, using Lipofectamine 2000 Reagent (Thermofisher, Massachusetts, USA). Six hours post-transfection, test compounds were added, and luciferase activity was measured 48 h later with the Dual-Luciferase Assay System. Firefly luciferase activity was normalized to Renilla luciferase activity. All experiments were repeated three times under the same conditions.

4.5. Western blot

Cell or tissue samples were lysed using a radio-immunoprecipitation assay buffer. Protein concentration in the samples was determined using the BCA Protein Assay Kit (Beyotime, Shanghai, China) according to the manufacturer's instructions. The protein solution was diluted with SDS-PAGE sample loading buffer (5 ×) containing the reducing reagent and heated at 95 °C for 5 min. Proteins were separated on 4–20 % SDS-polyacrylamide gels (Yeasen, Shanghai, China) and then transferred onto polyvinylidene fluoride (PVDF) membranes. The membranes were blocked with 5 % bovine serum albumin at 37 °C for 1 h, followed by overnight incubation with primary antibodies at 4 °C. After washing, the membranes were incubated with a secondary antibody at room temperature for 1 h and detected using Tanon5200. The primary antibodies used were mouse anti-α-SMA (Boster, Wuhan, China), rabbit anti-collagen I (Boster, Wuhan, China), and mouse anti-β-actin (Boster, Wuhan, China). Horseradish peroxidase-conjugated goat anti-rabbit/mouse IgG (Boster, Wuhan, China) was used as the secondary antibody. Images were acquired with Image Lab 6.0.1, and cumulative densitometric analyses of the Western blot images were performed using ImageJ 1.54a.

4.6. The CCl_4-induced mouse hepatic fibrosis model

Male C57BL/6 mice (8 weeks old) were obtained from the Medical School of Yangzhou University (Yangzhou, China). All animal experiments were conducted in strict compliance with the Guide for the Care and Use of Laboratory Animals of the National Institutes of Health and were approved by the Experimentation Ethics Review Committee of China Pharmaceutical University. The animals were housed in a specific-pathogen-free facility with a temperature of 24 ± 2 °C, humidity of 40–70 %, and a 12-h dark/light cycle. To establish the CCl_4-induced liver fibrosis model, mice received intraperitoneal injections of a CCl_4/corn oil (1/50, v/v) mixture at a dose of 0.5 mL/kg three times a week for 4 weeks. Treatments began after 2 weeks of CCl_4 injections, when fibrosis typically develops. DMSO, Calcipotriol (100 μg/kg body weight), compound **15a**, or **E15** (500 μg/kg body weight) was administered by oral gavage five times weekly for 2 weeks. Mice were sacrificed 4 h after the final treatment to collect serum and liver samples for blood chemistry analysis, immunofluorescence and histological staining, Western blot, and qPCR assays.

4.7. Blood chemistry analysis

To assess liver function changes in each group of mice, serum was obtained by centrifuging whole blood samples at 12,000 rpm for 10 min at 4 °C. The levels of serum alanine aminotransferase (ALT), aspartate transaminase (AST), total bile acid (TBA), and calcium were measured using commercial kits from Rayto (Shenzhen, China).

4.8. Histological staining

For histological staining, liver tissues were fixed in 4 % (w/v) neutral phosphate-buffered paraformaldehyde for 24 h, followed by dehydration, clearing, and embedding in paraffin. The tissues were then sectioned at a thickness of 5 μm and stained with hematoxylin-eosin (H&E) for structural observation, or with Masson's Trichrome staining to detect collagen deposits.

4.9. Statistical analysis

Data are expressed as means ± standard deviation (SD). Statistical significance was assessed using a two-tailed unpaired Student's t-test for comparisons between two sets of values or ANOVA for comparisons among multiple groups, utilizing GraphPad Prism 8. Exact P values are provided in the figures or their legends. No exclusion criteria were applied in the design of the experiments for this study.

4.10. Molecular docking

The docking experiments were conducted using the hVDR crystal structure (PDB ID: 7QPP). The protein structure was prepared using the Protein Preparation Wizard module with default parameters. The workflow included preprocessing the structure, optimizing hydrogen bonds, and performing restrained minimization. The ligand structures were prepared using the LigPrep module with default settings. Receptor grids were generated using the Receptor Grid Generation module, centering the grid on the co-crystallized ligand and employing default parameters. Docking was performed using the Ligand Docking module in extra precision (XP) mode with default settings.

CRediT authorship contribution statement

Fei Gao: Writing – original draft, Project administration, Methodology, Investigation. **Chun Guan:** Writing – original draft, Project administration, Methodology, Investigation. **Nuo Cheng:** Project administration, Methodology, Formal analysis. **Yichen Liu:** Validation, Methodology, Formal analysis, Data curation. **Yue Wu:** Methodology,

Investigation. **Bingyue Shi:** Project administration, Methodology. **Jiayi Huang:** Project administration, Methodology. **Sitong Li:** Methodology, Investigation. **Yu Tong:** Software, Project administration. **Yi Gao:** Methodology, Investigation. **Jiayi Liu:** Methodology. **Cong Wang:** Writing – review & editing, Validation, Supervision, Funding acquisition. **Can Zhang:** Supervision, Funding acquisition, Conceptualization.

Declaration of competing interest

The authors declare that they have no known competing financial interests or personal relationships that could have appeared to influence the work reported in this paper.

Acknowledgments

We thank the Public Platform of the State Key Laboratory of Natural Medicines for assistance with the pathological-section imaging. This work was supported by the National Natural Science Foundation of China (Nos. 92159304, 82130102, 81930099, 81773664, 81703585), the Natural Science Foundation of Jiangsu Province (No. BK20212011), the Natural Science Foundation of Chongqing (CSTB2023NSCQMSX0607), the "Open Competition to Select the Best Candidates" Key Technology Program for Nucleic Acid Drugs of NCTIB (No. NCTIB2022HS01014), the "Double First-Class" University Project (No. CPU2022QZ05), the Fundamental Research Funds for the Central Universities of China (No. 2632022ZD11), the National Innovation and Entrepreneurship Training Program for Undergraduate (No. 202410316039Z) and the Open Project of State Key Laboratory of Natural Medicines (No. SKLNMZZ202223).

Abbreviations used

VD, Vitamin D; VDR, Vitamin D receptor; LBD, Ligand binding domain; RXR, Retinol X receptor; VDRE, Vitamin D response element; HSCs, Hepatic stellate cells; ECM, Extracellular matrix; α-SMA, α-Smooth actin; TGF-β1, Transforming growth factor-β1; TIMP-1, Tissue inhibitor of metalloproteinase-1; CTGF, Connective tissue growth factor; SAR, Structure-activity relationship.

Appendix A. Supplementary data

Supplementary data to this article can be found online at https://doi.org/10.1016/j.ejmech.2025.117250.

Data availability

Data will be made available on request.

References

[1] G. Jones, Extrarenal vitamin D activation and interactions between vitamin D(2), vitamin D(3), and vitamin D analogs, Annu. Rev. Nutr. 33 (2013) 23–44, https://doi.org/10.1146/annurev-nutr-071812-161203.
[2] M.R. Haussler, C.A. Haussler, P.W. Jurutka, et al., The vitamin D hormone and its nuclear receptor: molecular actions and disease states, J. Endocrinol. 154 (3) (1997) S57–S73.
[3] R. Lin, J.H. White, The pleiotropic actions of vitamin D, Bioessays 26 (1) (2004) 21–28, https://doi.org/10.1002/bies.10368.
[4] M.R. Haussler, G.K. Whitfield, I. Kaneko, et al., Molecular mechanisms of vitamin D action, Calcif. Tissue Int. 92 (2) (2013) 77–98, https://doi.org/10.1007/s00223-012-9619-0.
[5] S. Chen, J. Cui, K. Nakamura, et al., Coactivator-vitamin D receptor interactions mediate inhibition of the atrial natriuretic peptide promoter, J. Biol. Chem. 275 (20) (2000) 15039–15048, https://doi.org/10.1074/jbc.275.20.15039.
[6] M.R. Haussler, P.W. Jurutka, J.C. Hsieh, et al., New understanding of the molecular mechanism of receptor-mediated genomic actions of the vitamin D hormone, Bone 17 (2) (1995) S33–S38, https://doi.org/10.1016/8756-3282(95)00205-R.
[7] E. Abe, C. Miyaura, H. Sakagami, et al., Differentiation of mouse myeloid leukemia cells induced by 1 alpha,25-dihydroxyvitamin D(3), Proc. Natl. Acad. Sci. USA 78 (8) (1981) 4990–4994, https://doi.org/10.1073/pnas.78.8.4990.
[8] A. Skrobot, U. Demkow, M. Wachowska, Immunomodulatory role of vitamin D, in: A. Review, M. Pokorski (Eds.), Current Trends in Immunity and Respiratory Infections, Springer International Publishing, Cham, 2018, pp. 13–23, https://doi.org/10.1007/5584_2018_246.
[9] S. Petta, C. Cammà, C. Scazzone, et al., Low vitamin D serum level is related to severe fibrosis and low responsiveness to interferon-based therapy in genotype 1 chronic hepatitis C, Hepatology 51 (4) (2010) 1158–1167, https://doi.org/10.1002/hep.23489.
[10] B. Terrier, F. Carrat, G. Geri, et al., Low 25-OH vitamin D serum levels correlate with severe fibrosis in HIV-HCV co-infected patients with chronic hepatitis, J. Hepatol. 55 (4) (2011) 756–761, https://doi.org/10.1016/j.jhep.2011.01.041.
[11] J. Arteh, S. Narra, S. Nair, Prevalence of vitamin D deficiency in chronic liver disease, Dig. Dis. Sci. 55 (9) (2010) 2624–2628, https://doi.org/10.1007/s10620-009-1069-9.
[12] K. Baur, J.C. Mertens, J. Schmitt, et al., Combined effect of 25-OH vitamin D plasma levels and genetic Vitamin D Receptor (NR 1I1) variants on fibrosis progression rate in HCV patients, Liver Int. 32 (4) (2012) 635–643, https://doi.org/10.1111/j.1478-3231.2011.02674.x.
[13] P. Komolmit, S. Kimtrakool, S. Suksawatamnuay, et al., Vitamin D supplementation improves serum markers associated with hepatic fibrogenesis in chronic hepatitis C patients: a randomized, double-blind, placebo-controlled study, Sci. Rep. 7 (1) (2017) 8905, https://doi.org/10.1038/s41598-017-09512-7.
[14] J.N. Artaza, K.C. Norris, Vitamin D reduces the expression of collagen and key profibrotic factors by inducing an antifibrotic phenotype in mesenchymal multipotent cells, J. Endocrinol. 200 (2) (2009) 207–221, https://doi.org/10.1677/JOE-08-0241.
[15] A. Beilfuss, J.-P. Sowa, S. Sydor, et al., Vitamin D counteracts fibrogenic TGF-β signalling in human hepatic stellate cells both receptor-dependently and independently, Gut 64 (5) (2015) 791–799, https://doi.org/10.1136/gutjnl-2014-307024.
[16] S. Abramovitch, L. Dahan-Bachar, E. Sharvit, et al., Vitamin D inhibits proliferation and profibrotic marker expression in hepatic stellate cells and decreases thioacetamide-induced liver fibrosis in rats, Gut 60 (12) (2011) 1728–1737, https://doi.org/10.1136/gut.2010.234666.
[17] K. Hochrath, C.S. Stokes, J. Geisel, et al., Vitamin D modulates biliary fibrosis in ABCB4-deficient mice, Hepatology International 8 (3) (2014) 443–452, https://doi.org/10.1007/s12072-014-9548-2.
[18] Puche J E, Saiman Y, Friedman S L: Hepatic Stellate Cells and Liver Fibrosis, Compr. Physiol.: 1473-1492. https://doi.org/10.1002/cphy.c120035.
[19] M. Gascon-Barré, C. Demers, A. Mirshahi, et al., The normal liver harbors the vitamin D nuclear receptor in nonparenchymal and biliary epithelial cells, Hepatology 37 (5) (2003) 1034–1042, https://doi.org/10.1053/jhep.2003.50176.
[20] N. Ding, Ruth t Yu, N. Subramaniam, et al., A vitamin D receptor/SMAD genomic circuit gates hepatic fibrotic response, Cell 153 (3) (2013) 601–613, https://doi.org/10.1016/j.cell.2013.03.028.
[21] A. Duran, Eloy d Hernandez, M. Reina-Campos, et al., p62/SQSTM1 by binding to vitamin D receptor inhibits hepatic stellate cell activity, fibrosis, and liver cancer, Cancer Cell 30 (4) (2016) 595–609, https://doi.org/10.1016/j.ccell.2016.09.004.
[22] X. Liu, Y. Wu, Y. Li, et al., Vitamin D receptor (VDR) mediates the quiescence of activated hepatic stellate cells (aHSCs) by regulating M2 macrophage exosomal smooth muscle cell-associated protein 5 (SMAP-5), J. Zhejiang Univ. - Sci. B 24 (3) (2023) 248–261.
[23] G. Jones, M. Kaufmann, Update on pharmacologically-relevant vitamin D analogues, Br. J. Clin. Pharmacol. 85 (6) (2019) 1095–1102, https://doi.org/10.1111/bcp.13781.
[24] C. Wang, B. Wang, L. Xue, et al., Design, synthesis, and antifibrosis activity in liver of nonsecosteroidal vitamin D receptor agonists with phenyl-pyrrolyl pentane skeleton, J. Med. Chem. 61 (23) (2018) 10573–10587, https://doi.org/10.1021/acs.jmedchem.8b01165.
[25] K. Xing, Y. Wu, F. Gao, et al., Design, synthesis and anti-hepatic fibrosis activity of novel diphenyl vitamin D receptor agonists, Eur. J. Med. Chem. 258 (2023) 115596, https://doi.org/10.1016/j.ejmech.2023.115596.
[26] N. Rochel, J.M. Wurtz, A. Mitschler, et al., The crystal structure of the nuclear receptor for vitamin D bound to its natural ligand, Mol. Cell 5 (1) (2000) 173–179, https://doi.org/10.1016/S1097-2765(00)80413-X.
[27] M.R. Haussler, G.K. Whitfield, I. Kaneko, et al., Molecular mechanisms of vitamin D action, Calcif. Tissue Int. 92 (2) (2013) 77–98, https://doi.org/10.1007/s00223-012-9619-0.
[28] A. Verstuyf, L. Verlinden, E. Van Etten, et al., Biological activity of CD-ring modified 1α,25-dihydroxyvitamin D analogues: C-ring and five-membered D-ring analogues, J. Bone Miner. Res. 15 (2) (2010) 237–252, https://doi.org/10.1359/jbmr.2000.15.2.237.
[29] C. Carlberg, F. Molnár, A. Mouriño, Vitamin D receptor ligands: the impact of crystal structures, Expert Opin. Ther. Pat. 22 (4) (2012) 417–435, https://doi.org/10.1517/13543776.2012.673590.
[30] S. Seoane, P. Gogoi, A. Zárate-Ruíz, et al., Design, synthesis, biological activity, and structural analysis of novel Des-C-ring and aromatic-D-ring analogues of 1α,25-dihydroxyvitamin D_3, J. Med. Chem. 65 (19) (2022) 13112–13124, https://doi.org/10.1021/acs.jmedchem.2c00900.
[31] A. Zárate-Ruíz, S. Seoane, C. Peluso-Iltis, et al., Further studies on the highly active Des-C-ring and aromatic-D-ring analogues of 1α,25-dihydroxyvitamin D_3 (calcitriol): refinement of the side chain, J. Med. Chem. 66 (22) (2023) 15326–15339, https://doi.org/10.1021/acs.jmedchem.3c01371.
[32] M. Takano, D. Sawada, K. Yasuda, et al., Synthesis and metabolic studies of 1α,2α,25-, 1α,4α,25- and 1α,4β,25-trihydroxyvitamin D(3), J. Steroid Biochem. Mol. Biol. 148 (2015) 34–37, https://doi.org/10.1016/j.jsbmb.2014.09.021.

[33] Y. Sasaki, Y. Horita, C. Zhong, et al., Copper(I)-Catalyzed regioselective monoborylation of 1,3-enynes with an internal triple bond: selective synthesis of 1,3-dienylboronates and 3-Alkynylboronates, Angew. Chem. Int. Ed. 50 (12) (2011) 2778–2782, https://doi.org/10.1002/anie.201007182.
[34] J.W. Pike, M.B. Meyer, The vitamin D receptor: new paradigms for the regulation of gene expression by 1,25-dihydroxyvitamin D3, Rheum. Dis. Clin. N. Am. 38 (1) (2012) 13–27, https://doi.org/10.1016/j.rdc.2012.03.004.
[35] L. Xu, A.Y. Hui, E. Albanis, et al., Human hepatic stellate cell lines, LX-1 and LX-2: new tools for analysis of hepatic fibrosis, Gut 54 (1) (2005) 142–151, https://doi.org/10.1136/gut.2004.042127.
[36] K. Wang, S. Fang, Q. Liu, et al., TGF-β1/p65/MAT2A pathway regulates liver fibrogenesis via intracellular SAM, EBioMedicine 42 (2019) 458–469, https://doi.org/10.1016/j.ebiom.2019.03.058.
[37] C.-C. Tsai, S.-B. Wu, H.-C. Kau, et al., Essential role of connective tissue growth factor (CTGF) in transforming growth factor-β1 (TGF-β1)-induced myofibroblast transdifferentiation from Graves' orbital fibroblasts, Sci. Rep. 8 (1) (2018) 7276, https://doi.org/10.1038/s41598-018-25370-3.
[38] S.-A. Park, M.-J. Kim, S.-Y. Park, et al., TIMP-1 mediates TGF-β-dependent crosstalk between hepatic stellate and cancer cells via FAK signaling, Sci. Rep. 5 (1) (2015) 16492, https://doi.org/10.1038/srep16492.
[39] B.M. Wu, J.D. Liu, Y.H. Li, et al., Margatoxin mitigates CCl4-induced hepatic fibrosis in mice via macrophage polarization, cytokine secretion and STAT signaling, Int. J. Mol. Med. 45 (1) (2020) 103–114, https://doi.org/10.3892/ijmm.2019.4395.
[40] C. Solomon, M. Macoritto, X.L. Gao, et al., The unique tryptophan residue of the vitamin D receptor is critical for ligand binding and transcriptional activation, J. Bone Miner. Res. 16 (1) (2009) 39–45, https://doi.org/10.1359/jbmr.2001.16.1.39.